



# Broadly effective metabolic and immune recovery with C5 inhibition in CHAPLE disease

Ahmet Ozen<sup>1,2,3</sup>✉, Nurhan Kasap<sup>1,2,3</sup>, Ivan Vujkovic-Cvijin<sup>4</sup>, Richard Apps<sup>5</sup>, Foo Cheung<sup>5</sup>, Elif Karakoc-Aydiner<sup>1,2,3</sup>, Bilge Akkelle<sup>6</sup>, Sinan Sari<sup>7</sup>, Engin Tutar<sup>6</sup>, Figen Ozcay<sup>8</sup>, Dilara Kocacik Uygun<sup>9</sup>, Ali Islek<sup>10</sup>, Gamze Akgun<sup>2,3,11</sup>, Merve Selcuk<sup>12</sup>, Oya Balci Sezer<sup>8</sup>, Yu Zhang<sup>13,14</sup>, Günsel Kutluk<sup>15</sup>, Erdem Topal<sup>16</sup>, Ersin Sayar<sup>17</sup>, Cigdem Celikel<sup>18</sup>, Roderick H. J. Houwen<sup>19</sup>, Aysen Bingol<sup>9</sup>, Ismail Ogulur<sup>1,2,3</sup>, Sevgi Bilgic Eltan<sup>2,3,11</sup>, Andrew L. Snow<sup>20</sup>, Camille Lake<sup>20</sup>, Giovanna Fantoni<sup>5</sup>, Camille Alba<sup>21</sup>, Brian Sellers<sup>5</sup>, Samuel D. Chauvin<sup>14,22</sup>, Clifton L. Dalgard<sup>23</sup>, Olivier Harari<sup>24</sup>, Yan G. Ni<sup>24</sup>, Ming-Dauh Wang<sup>24</sup>, Kishor Devalaraja-Narashimha<sup>24</sup>, Poorani Subramanian<sup>14,25</sup>, Rabia Ergelen<sup>26</sup>, Reha Artan<sup>27</sup>, Sukru Nail Guner<sup>28</sup>, Buket Dalgic<sup>7</sup>, John Tsang<sup>5</sup>, Yasmine Belkaid<sup>14,5</sup>, Deniz Ertem<sup>6</sup>, Safa Baris<sup>1,2,3</sup> and Michael J. Lenardo<sup>14,22</sup>✉

**Complement hyperactivation, angiopathic thrombosis and protein-losing enteropathy (CHAPLE disease) is a lethal disease caused by genetic loss of the complement regulatory protein CD55, leading to overactivation of complement and innate immunity together with immunodeficiency due to immunoglobulin wasting in the intestine. We report in vivo human data accumulated using the complement C5 inhibitor eculizumab for the medical treatment of patients with CHAPLE disease. We observed cessation of gastrointestinal pathology together with restoration of normal immunity and metabolism. We found that patients rapidly renormalized immunoglobulin concentrations and other serum proteins as revealed by aptamer profiling, re-established a healthy gut microbiome, discontinued immunoglobulin replacement and other treatments and exhibited catch-up growth. Thus, we show that blockade of C5 by eculizumab effectively re-establishes regulation of the innate immune complement system to substantially reduce the pathophysiological manifestations of CD55 deficiency in humans.**

In 1961, T. A. Waldmann described serum hypoproteinemia associated with protein-losing enteropathy (PLE)<sup>1</sup>. The disease pathogenesis was unknown, and temporizing measures such as albumin infusions and immunoglobulin replacement therapy

(IgRT) became the conventional therapies. In 2017, the discovery of 'CD55 deficiency with hyperactivation of complement, angiopathic thrombosis, and PLE' (CHAPLE disease, MIM 226300) revealed that complement and innate immunity hyperactivation caused by

<sup>1</sup>Division of Allergy and Immunology, Department of Pediatrics, School of Medicine, Marmara University, Istanbul, Turkey. <sup>2</sup>Istanbul Jeffrey Modell Diagnostic Center for Primary Immunodeficiency Diseases, Istanbul, Turkey. <sup>3</sup>The Isil Berat Barlan Center for Translational Medicine, Istanbul, Turkey. <sup>4</sup>Metaorganism Immunity Section, Laboratory of Immune System Biology, National Institute of Allergy and Infectious Diseases (NIAID), National Institutes of Health (NIH), Bethesda, MD, USA. <sup>5</sup>Trans-NIH Center for Human Immunology, Autoimmunity, and Inflammation, NIH, Bethesda, MD, USA. <sup>6</sup>Division of Gastroenterology, Hepatology and Nutrition, Department of Pediatrics, School of Medicine, Marmara University, Istanbul, Turkey. <sup>7</sup>Division of Gastroenterology, Hepatology and Nutrition, Department of Pediatrics, School of Medicine, Gazi University, Ankara, Turkey. <sup>8</sup>Division of Gastroenterology, Hepatology and Nutrition, Department of Pediatrics, Baskent University Hospital, Ankara, Turkey. <sup>9</sup>Division of Allergy and Immunology, Department of Pediatrics, School of Medicine, Akdeniz University, Antalya, Turkey. <sup>10</sup>Division of Gastroenterology, Hepatology and Nutrition, Department of Pediatrics, Ataturk University, Erzurum, Turkey. <sup>11</sup>Division of Allergy and Immunology, Department of Pediatrics, Ministry of Health, Marmara University, Istanbul, Turkey. <sup>12</sup>Department of Pediatrics, School of Medicine, Marmara University, Istanbul, Turkey. <sup>13</sup>Human Immunological Diseases Section, Laboratory of Clinical Immunology and Microbiology, NIAID, NIH, Bethesda, MD, USA. <sup>14</sup>Clinical Genomics Program, NIAID, NIH, Bethesda, MD, USA. <sup>15</sup>Division of Gastroenterology, Hepatology and Nutrition, Department of Pediatrics, Kanuni Sultan Süleyman Training and Research Hospital, Health Sciences University, Istanbul, Turkey. <sup>16</sup>Division of Allergy and Immunology, Department of Pediatrics, School of Medicine, Inonu University, Malatya, Turkey. <sup>17</sup>Division of Gastroenterology, Hepatology and Nutrition, Department of Pediatrics, Alanya Alaaddin Keykubat University, Alanya, Turkey. <sup>18</sup>Department of Pathology, School of Medicine, Marmara University, Istanbul, Turkey. <sup>19</sup>Department of Pediatric Gastroenterology, University Medical Center–Wilhelmina Children's Hospital, Utrecht, the Netherlands. <sup>20</sup>Department of Pharmacology and Molecular Therapeutics, Uniformed Services University of the Health Sciences, Bethesda, MD, USA. <sup>21</sup>The American Genome Center, Henry Jackson Foundation, Uniformed Services University of Health Sciences, Bethesda, MD, USA. <sup>22</sup>Molecular Development of the Immune System Section and NIAID Clinical Genomics Program, Laboratory of Immune System Biology, NIAID, NIH, Bethesda, MD, USA. <sup>23</sup>Department of Anatomy, Physiology and Genetics, The American Genome Center, Uniformed Services University of the Health Sciences, Bethesda, MD, USA. <sup>24</sup>Regeneron Pharmaceuticals, Inc, Tarrytown, NY, USA. <sup>25</sup>Bioinformatics and Computational Biosciences Branch, Office of Cyber Infrastructure and Computational Biology, NIAID, NIH, Bethesda, MD, USA. <sup>26</sup>Department of Radiology, School of Medicine, Marmara University, Istanbul, Turkey. <sup>27</sup>Division of Pediatric Gastroenterology, Hepatology and Nutrition, Department of Pediatrics, School of Medicine, Akdeniz University, Antalya, Turkey. <sup>28</sup>Division of Pediatric Allergy and Immunology, Meram Medical Faculty, Necmettin Erbakan University, Konya, Turkey. ✉e-mail: [ahmet.ozen@marmara.edu.tr](mailto:ahmet.ozen@marmara.edu.tr); [lenardo@nih.gov](mailto:lenardo@nih.gov)

CD55 (also known as decay acceleration factor) gene deficiency can cause this disorder<sup>2,3</sup>. The cardinal features are severe PLE due to primary intestinal lymphangiectasia due to the inflammatory attack on intestinal lymphatic vessels by complement and innate immune overactivation<sup>2,4</sup>. CHAPLE leads to severe pathophysiology, including diarrhea with protein-wasting, vomiting, abdominal pain and edema that cause a metabolic starvation state; recurrent infections due to hypogammaglobulinemia; and severe, often fatal, thromboembolic complications<sup>1,2,4</sup>. The disease occurs globally but prevails in areas with high consanguinity, such as the Iğdir region of eastern Turkey, where there is a high carrier frequency of *CD55* loss of function alleles. Lethal CHAPLE disease, ‘tedirgin’ in the local language (meaning agitated), is prevalent there, and desperate parents of affected children resort to folk remedies since conventional therapies do not improve or extend life. Thus, understanding the immune and metabolic derangements due to *CD55* loss and how they change with complement interventions is critical.

The complement system is a cascade of proteins coordinated with innate and adaptive immunity to destroy pathogens and clear immune complexes, apoptotic cells and debris<sup>5,6</sup>. Complement activation produces bioactive peptides—anaphylatoxins—that can alter both innate and adaptive immune responses and leads to the assembly of a membrane attack complex (MAC) that can lyse targets such as pathogens or cells<sup>7</sup>. Unwanted complement activation on host/self cells is regulated by the cell surface glycoproteins *CD55* (decay acceleration factor), *CD46* and *CD59*, which protect normal hematopoietic, endothelial and epithelial cells from complement-mediated damage<sup>8</sup>. In the gastrointestinal (GI) tract, lymph recirculation through lymph vessels called lacteals return serum proteins such as albumin and immunoglobulin to venous circulation. The genetic loss of *CD55* induces local complement hyperactivation that deposits MAC on GI lymphatics, causing PLE<sup>2</sup>. Other severe diseases, such as paroxysmal nocturnal hemoglobinuria (PNH) and atypical hemolytic uremic syndrome, result from the loss of complement inhibitors and uncontrolled complement activation on erythrocytes and kidney basal membrane cells, respectively<sup>2,9–12</sup>. Both conditions are treated effectively with the complement inhibitor eculizumab (Soliris). Eculizumab is a monoclonal antibody that binds to and inhibits the activation of C5, which occurs normally as consequence of the activation of the central complement component C3. *CD55* is a negative regulator of the C3 and C5 convertases that mediate cleavage activation of C3 and C5. We found that eculizumab successfully abrogated complement activation *in vitro* in T cells from patients with CHAPLE disease<sup>2</sup>.

Previous studies reported that eculizumab improved the condition of three members of a family with *CD55* deficiency<sup>3,13</sup>. These promising results raised several important questions. Would eculizumab have broad efficacy in families with different genetic backgrounds and *CD55* mutations? What physiological manifestations of disease would be alleviated, and would healthy immunity and

metabolism be re-established. What are the drug pharmacokinetics and pharmacodynamics for complement control? Are there pharmacogenomic variants that determine treatment efficacy and dosing? Because PLE causes a starvation state, what are the specific metabolic effects of the disease and treatment? Multiplexed proteomic platforms have identified new biomarkers and new disease mechanisms. For example, the investigation of inflammatory bowel disease using ‘slow off-rate modified aptamers’ (SOMAmers) revealed key serum protein changes independent of transcriptome changes, suggesting this could help elucidate CHAPLE disease mechanisms<sup>14</sup>. Finally, despite ubiquitous *CD55* expression in the body, the severe complement hyperactivation in CHAPLE disease affects mainly the GI tract. Could microbiome studies yield insights into GI pathogenesis?<sup>15,16</sup> We therefore comprehensively investigated eculizumab as a medical treatment in patients with CHAPLE disease with different *CD55* gene mutations.

## Results

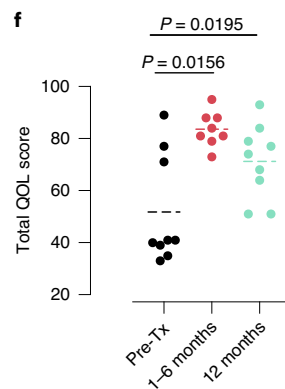
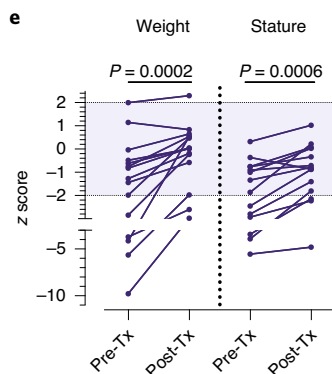
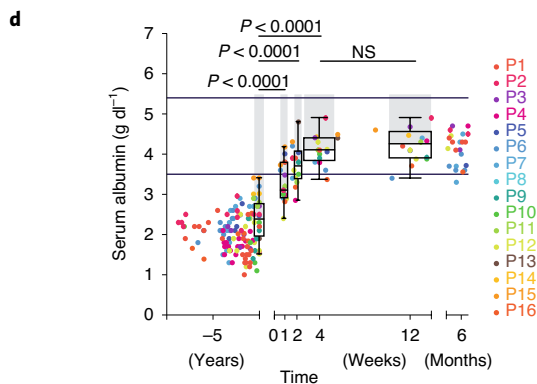
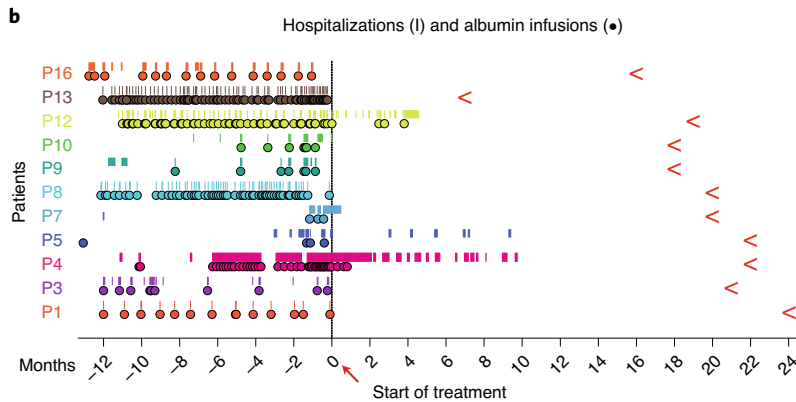
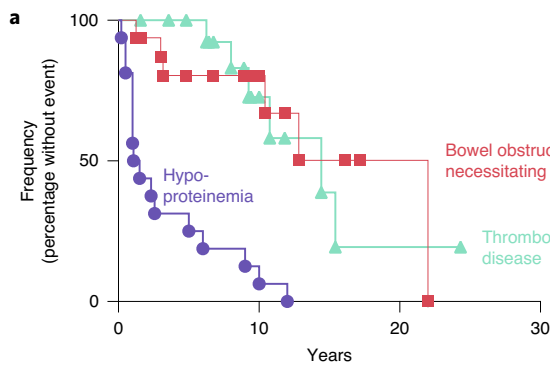
**Natural history of a case series of CHAPLE disease.** We evaluated 16 patients with CHAPLE disease from 14 families diagnosed with recessive biallelic *CD55* gene mutations causing decreased *CD55* expression and complement overactivation (Extended Data Fig. 1 and Supplementary Fig. 1)<sup>2</sup>. All patients manifested severe PLE leading to hypoproteinemia, low immunoglobulin concentrations and recurrent infections, abdominal pain, nausea, vomiting, diarrhea, loss of appetite, weight loss and edema (Extended Data Figs. 1 and 2 and Supplementary Information)<sup>2,3</sup>. Patients progressed to three life-threatening conditions: hypoproteinemia causing metabolic derangements, starvation and infections; debilitating GI inflammation, ulceration and obstruction; and severe, often fatal, thromboembolic disease (Fig. 1a, Extended Data Fig. 2 and Supplementary Information, case histories). Patients required frequent hospitalizations and many medical interventions, including albumin infusions and IgRT, that failed to alleviate disease (Fig. 1b and Extended Data Fig. 3). In the extended families, we found 32 probable patients with CHAPLE disease, of whom 8 died in childhood (25%) and many others were severely ill.

**Eculizumab causes rapid improvement in most symptoms and overall health.** During medical care, we filed appeals to the Turkish Medicines and Medical Devices Agency to provide eculizumab not as a clinical trial but for off-label use in the care of each of the 15 patients. The 16th patient was treated in the Netherlands using eculizumab provided by medical insurance. We observed treatment effects over a median of 20 months (interquartile range 18–22 months) totaling 309 patient–months of data. Strikingly, most patients no longer required hospitalization or transfusions of albumin or immunoglobulin following eculizumab therapy (Fig. 1b). Three patients did not receive the full regimen due to inaccessibility (patient (P) 5) or medical reasons (P12), or there was only a partial

**Fig. 1 | The treatment effect of eculizumab in CHAPLE disease.** **a**, A Kaplan–Meier plot showing the cumulative frequency of being without hypoproteinemia (purple), bowel obstruction (red) and thromboembolic disease (green) versus time (years) ( $n=16$ ). **b**, Timeline of hospitalizations (vertical line) and albumin infusions (circles) for 11 patients pretreatment (pre-Tx) (–) and post-treatment (post-Tx) (+) (months). Red leftward arrowheads indicate the end of the observation period. **c**, Heatmaps of the prevalence (percentage of patients,  $n=16$ ) in the study population of the indicated clinical parameter or therapeutic intervention, respectively, over patient lifetime (past), past year pre-Tx and the post-Tx observation period when a particular patient has been on regular eculizumab treatment. **d**, Serum albumin concentration before and after treatment beginning at  $t=0$ . Horizontal bars show normal range; gray bars indicate statistical comparison range using mixed-effects analysis with Tukey’s multiple comparisons correction ( $n=16$ ). The statistical comparison of 4 versus 12 weeks revealed an adjusted  $P$  value of 0.3905 (NS, not significant). For each timepoint, the box plot shows the median, interquartile range and minimum and maximum values. **e**, Plots of weight and height (stature)  $z$ -scores compared to population averages pre-Tx and after 20 months of treatment using a paired  $t$ -test ( $n=12$ ). Gray region indicates the normal range.  $Z$ -scores were calculated using an online calculator (<https://peditools.org/growthpedi/index.php>) that uses Centers for Disease Control and Prevention (CDC) data tables as the chart source. **f**, Total QOL score of patients using the KINDL-R questionnaire ( $n=9$  for pre-Tx and 12 months’ assessments;  $n=8$  at 1–6 months). The statistical comparisons were made by Wilcoxon matched-pairs signed-rank test. All  $P$  values are two-sided. MCT, medium-chain triglyceride; TNF, tumor necrosis factor; TPA, tissue plasminogen activator.

drug response (P4 and Supplementary Information); however, all three responded to treatment adjustments. Long-standing pathophysiological signs and symptoms were eliminated by eculizumab (Fig. 1c and Extended Data Figs. 1 and 2). Most previous treatment interventions became unnecessary (Fig. 1c and Extended Data Fig. 3). However, supplementation of iron and vitamin D, thyroxin, anti-

coagulants and thrombolytic medications continued to be needed by some patients. Within months, the children exhibited a healthier appearance and function. Serum albumin increased into the normal range within 2–4 weeks, and remained normal at least 6 months or longer (Fig. 1d and Extended Data Fig. 1). The patients' heights and weights improved, and the total quality of life (QOL) scores



**c**

Clinical feature	Past year, Pre-Tx		
	Past	Past year, Pre-Tx	Post-Tx
Abdominal pain	100	100	0
Nausea	88	88	0
Vomiting	88	88	0
Diarrhea	88	86	0
Loss of appetite	75	75	0
Edema	88	88	0
Albumin transfusion	94	69	6
Thromboembolism	38	38	25
Thrombocytosis	80	88	6
Bowel obstruction	38	50	0
Low albumin	100	100	0
Low total protein	100	100	0
Low IgG	100	100	6
Low vitamin B12	80	73	0

**Intervention**

	Past	Past year, Pre-Tx	Post-Tx
Bowel resection surgery	33	6	0
Other invasive interventions	20	13	0
Multivitamins	67	50	0
Vitamin D	93	81	25
Vitamin B12	80	50	6
Folate	27	13	0
Iron	87	69	25
Calcium, magnesium, zinc	67	50	0
Omega-3 fatty acid	27	13	0
MCT oil	33	38	0
Enteral formula feeding	60	44	0
Parenteral nutrition	27	19	0
Erythrocyte transfusion	27	6	0
Albumin transfusion	93	69	0
Immunoglobulin Rx	60	56	0
Corticosteroids	87	63	0
Mesalazine	60	31	0
Azathioprine	47	19	0
Methotrexate	13	13	0
Anti-TNF	33	19	0
Low-molecular-weight heparin	14	25	19
Low-dose acetyl salicylic acid	20	31	13
TPA lysis of clots	7	6	6
Respiratory support	13	6	6
Octreotide to alleviate PLE	33	25	0
Antibiotic prophylaxis	53	31	0
Tx for unusual infections	53	38	0
Thyroxin for hypothyroidism	27	13	13

increased (Fig. 1e,f, Extended Data Fig. 2 and Supplementary Figs. 2 and 3). However, thrombocytosis, thrombosis and pulmonary embolism persisted in some patients (Fig. 1c and Extended Data Fig. 2). Overall, eculizumab treatment substantially restored normal physiology and immunity.

CHAPLE disease involves complement damage to GI lymphatics, so we evaluated the intestinal mucosa by endoscopy<sup>2</sup>. We found that lymphangiectasia, reflected by the dense white aggregates imparting a grayish cast on the mucosa, was eliminated by treatment (Fig. 2a). Eculizumab also promoted the healing of mucosal ulcers (Supplementary Fig. 4). Prospective symptom diaries revealed that the treatment reduced all GI symptoms and edema within 4 weeks (Fig. 2b, Extended Data Fig. 2 and Supplementary Fig. 5). Restoration of normal alimentary function was illustrated by increases in vitamin B12 and serum immunoglobulin, making IgRT and vitamin supplements unnecessary (Fig. 2c,d and Extended Data Fig. 1). We found markedly improved immune function, with reduced and less severe infections. Patients with CHAPLE disease also have abnormal increases in triglycerides and platelets that were reversed by eculizumab (Fig. 2e,f). Moreover, a blood cell aggregation abnormality was also eliminated by treatment (Fig. 2g). Radiological abnormalities, including bowel wall thickening, contrast enhancement, intestinal stricture and proximal dilatation, free fluid collection and abscess formation, also resolved with treatment (Fig. 2h). However, eculizumab therapy did not correct thromboembolic disease in P4, P7 and P14, or ischemic gliotic foci in P12. Thus, eculizumab effectively ameliorated most disease findings except for thromboembolic disease.

#### Dosing intervals, interrupted therapy and pharmacokinetics.

We next studied the pharmacokinetics and pharmacodynamics of eculizumab and total C5 (free + eculizumab bound). In a previous report, Kurolap et al. used an augmented induction regimen to account for GI protein-wasting with twice-weekly injections<sup>13</sup>. However, we found that once-weekly induction doses achieved a median trough concentration of eculizumab of 217 and 330  $\mu\text{g ml}^{-1}$ , at week 1 and weeks 2–4, respectively, which were much greater than 100  $\mu\text{g ml}^{-1}$ , the minimum recommended concentration (Fig. 3a). Eculizumab complexed with C5 to increase the total C5 (free + eculizumab bound) in the blood to a median of 219  $\mu\text{g ml}^{-1}$  (Fig. 3b). Even with the first dose, the eculizumab and total C5 concentrations reached  $\sim 200 \mu\text{g ml}^{-1}$  and were stable with the maintenance doses (Fig. 3a,b). We also observed that if dosing was delayed, eculizumab and total C5 concentrations fell slowly and reached baseline at 35 days (Fig. 3a,b). Total C5 for all patients reached a plateau when eculizumab reached 60–100  $\mu\text{g ml}^{-1}$  and the ratio of total C5 to eculizumab dropped below 2:1 (the theoretical ratio at which C5 becomes saturated by eculizumab) at 100  $\mu\text{g ml}^{-1}$  eculizumab (Fig. 3c and Supplementary Fig. 6a). We therefore tested

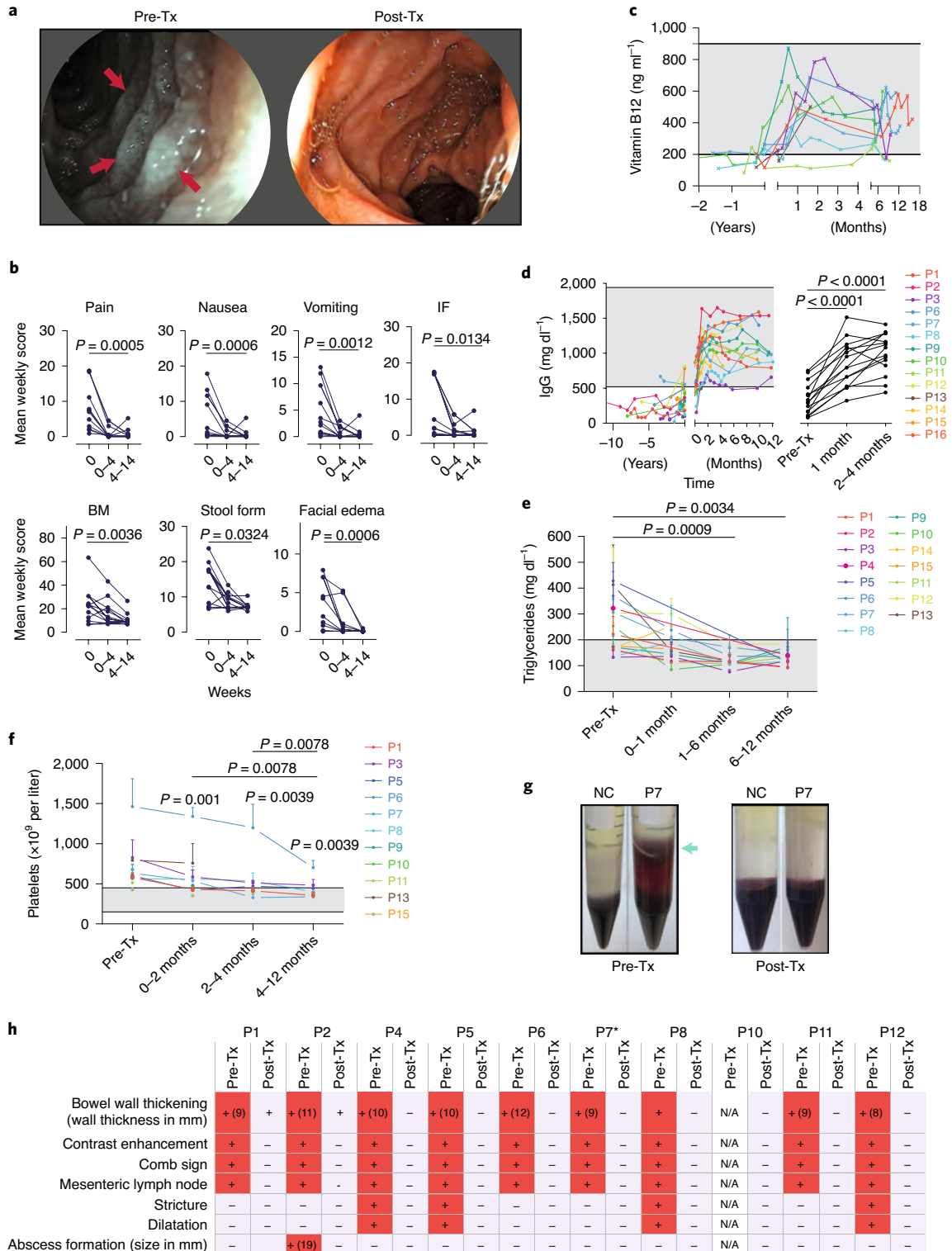
the activity of the classic complement pathway, employing the total hemolytic complement (CH50) test, and found it was completely inhibited by eculizumab  $> 100 \mu\text{g ml}^{-1}$  (Fig. 3d). Both the AH50 and CH50, measuring the target lysis-inducing activity of the alternative and classical pathways, respectively, were correlated with eculizumab concentrations and strongly suppressed at 1 week (Fig. 3e and Supplementary Fig. 6b,c). If dosing was delayed, eculizumab and total C5 concentrations progressively decreased, and AH50 and CH50 test value outcomes progressively increased with time (Fig. 3f and Extended Data Fig. 4). Thus, eculizumab rapidly and potentially inhibits uncontrolled complement activation and reverses PLE in vivo.

We also tried extended dosing intervals<sup>11,12</sup>. Using 4-week dosing, we found no disease relapse in P1, P3, P5, P8, P9, P10 and P11 (Extended Data Figs. 4 and 5a). By contrast, P4, the most severely affected in our cohort, showed disease relapse unless we used a 10-day dosing interval (Extended Data Fig. 5b). This finding was not explained by the CD55 mutation in P4, since the identical amino acid change is present in P2 and P5, who responded normally to eculizumab (Extended Data Fig. 1). In P4, we observed less CH50 and AH50 inhibition at comparable concentrations of serum eculizumab than in other patients (Fig. 3d,e). Also, total C5 accumulation was much higher in P4, suggesting eculizumab bound to C5 (Fig. 3b,c). We, therefore, performed whole-genome sequencing (WGS) on P4 and his affected sister, P5, who had responded better to treatment. We detected no new or extremely rare variants but a single-nucleotide polymorphism (SNP) (rs17611) encoding a V802I amino acid substitution in C5 that was homozygous in P4 and heterozygous in P5. This SNP is common (minor allele frequency = 0.4590 in the gnomAD database) with global homozygosity of about 23% (32,516 homozygous in 141,333 total individuals, [https://gnomad.broadinstitute.org/variant/9-123769200-C-T?dataset=gnomad\\_r2\\_1](https://gnomad.broadinstitute.org/variant/9-123769200-C-T?dataset=gnomad_r2_1)) and previously associated with inflammatory diseases, including liver fibrosis and rheumatoid arthritis<sup>17,18</sup>. The substituted residue is outside of the eculizumab binding site but alters the structure so that five new amino acid clashes occur in the complex (Supplementary Fig. 7a–c)<sup>19</sup>. Further genotyping showed that P8, P13 and P14 were also homozygous for I802 (Supplementary Fig. 7d). These patients had comparatively higher antibody–C5 complex concentrations, reduced C5a and slightly higher soluble C5b–9 complex (sC5b–9) but did not require increased administration of eculizumab (Supplementary Fig. 7e–g). Previous in vitro work showed that eculizumab blocks C5<sub>1802</sub> activity, but the variant protein is cleaved less efficiently by human neutrophil elastase<sup>17,20</sup>. Taken together, the C5<sub>802I/802I</sub> variant appears to alter the antibody–C5 complex and possibly its turnover<sup>21</sup>; however, more complicated factors are likely involved in the poor response of P4 to eculizumab therapy.

**Fig. 2 | GI, circulatory, hematologic and metabolic manifestations of CHAPLE disease with or without eculizumab.** **a**, Duodenal endoscopy images pre-Tx showing white lymph globules due to lymphangiectasia (red arrows) and lymph leakage imparting a grayish color to the mucosa and after 14 months of treatment showing lymphangiectasia replaced by normal mucosa. **b**, Mean total weekly scores as defined in the Methods for the indicated parameters in each patient during the pre-Tx (0), 0–4 weeks and 4–14 weeks post-Tx periods are plotted. Statistics used the Friedman test and Dunn's multiple comparisons test (two-sided *P* value; *n* = 13 patients at each timepoint). IF, inability to feed; BM, number of bowel movements. **c**, Vitamin B12 concentration in serum before and after treatment beginning at *t* = 0 (*n* = 9). **d**, Serum IgG concentration before and after treatment beginning at *t* = 0 (*n* = 15 for pre-Tx and 2–4 month assessments; *n* = 13 for 1 month assessment). **e**, Calculated mean and standard deviation for intrapatient repeated measurements of fasting blood triglyceride concentrations during pre-Tx periods or the indicated number of months post-Tx for each patient (*n* = 15). In **d** and **e**, statistical comparisons were made by mixed-effects analysis and Dunnett's multiple comparisons test (two-sided *P* value). **f**, Mean and s.d. values for multiple platelet count measurements obtained in each patient during the pre-Tx period or the indicated number of months post-Tx. Two-sided *P* values are calculated from Wilcoxon matched-pairs signed-rank test, based on the calculated means of multiple measurements for a given interval (*n* = 11 patients). **g**, Photographs of representative pre-Tx samples from P7 or normal control (NC) showing erythrocytes abnormally infiltrating the supernatant (arrow) during Ficoll gradient separation of PBMCs and disappearance of this phenotype post-Tx. **h**, Summary of radiological features before and after treatment. Red (+) shows presence of the sign and light blue (–) indicates absence. N/A, radiological studies not available. The asterisk in P7 indicates the presence of voluminous abdominal fluid before therapy that resolved following treatment (not shown). Shaded areas in **c–f** show normal range.

Eculizumab therapy was interrupted due to medication inaccessibility (P3 and P8) or a medical decision because of myocarditis (P12), and all experienced disease relapse (Extended Data Fig. 5c, Supplementary Fig. 8 and Supplementary Information). Thus, ongoing eculizumab therapy is necessary to sustain remission. Hence, CHAPLE disease differs from previous diseases in which the treatment can be tapered and discontinued<sup>22</sup>.

**Complement markers before and during eculizumab treatment.** Because complement variations contribute to disease variability, we assessed blood concentrations of C3, C4 and C5, and their activation products together with copy number variations (CNV) in the C4 gene (Fig. 4a–j)<sup>23</sup>. We observed C3a, C4b, C5a and soluble terminal complex (sC5b–9) were increased and complement Factor H (CFH) was decreased in baseline disease compared to age-matched



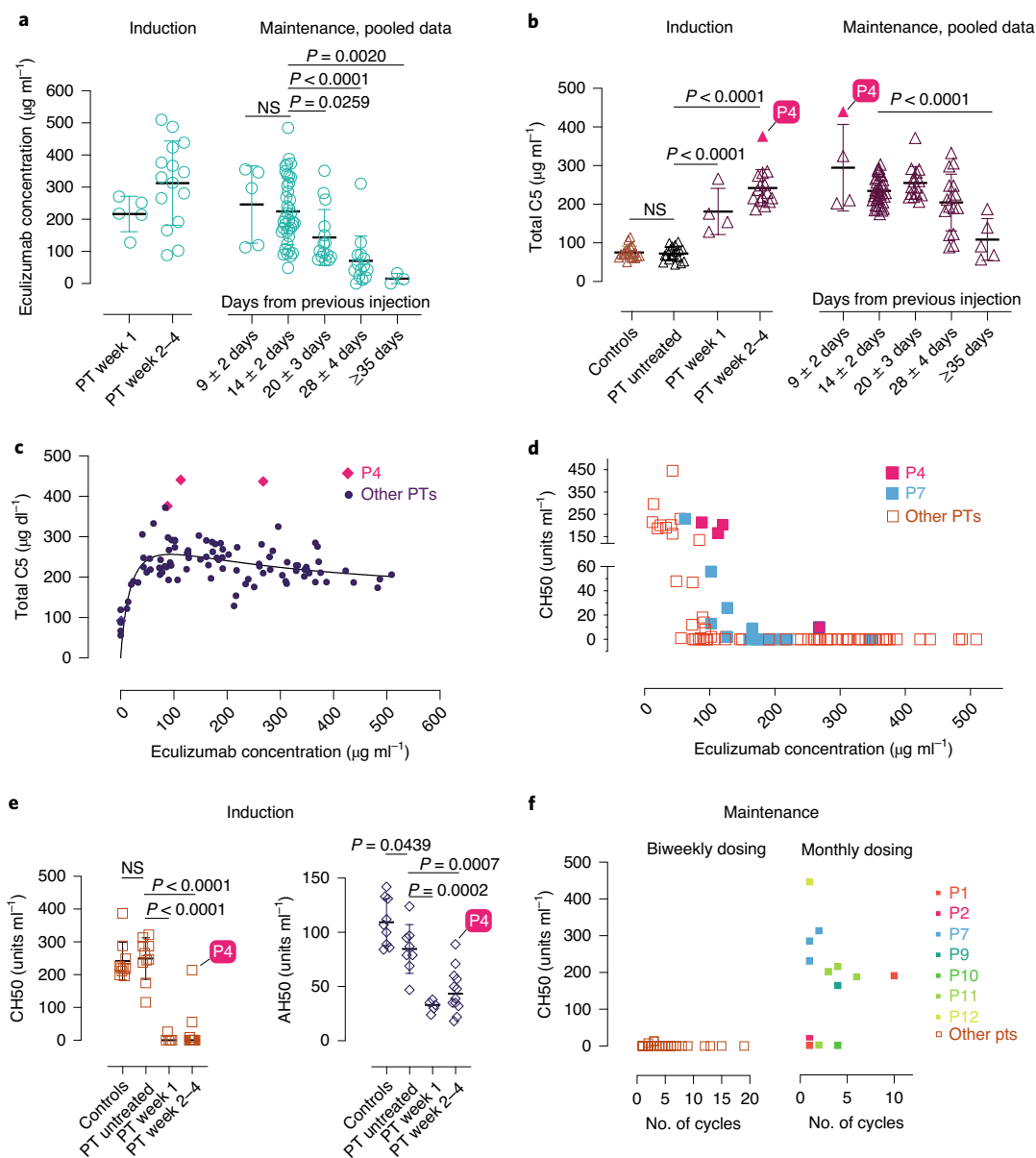


**Fig. 3 | Serum eculizumab concentration and total C5 and functional complement inhibition during the induction and maintenance phases of treatment.** **a,b**, Eculizumab and total C5 concentrations with respect to timing of therapy during the periods indicated. The respective exact  $P$  values comparing  $9 \pm 2$  and  $14 \pm 2$  days was 0.9803 in **a** and comparing controls and untreated patients was 0.9926 in **b**. **c,d**, Pooled analyses of patient samples showing total C5 (**c**) and CH50 (**d**) levels across the range of eculizumab concentrations. **e**, CH50 and AH50 levels with respect to timing of therapy during the periods indicated. **f**, CH50 values with respect to number of cycles on the standard biweekly dosing intervals or the modified monthly dosing regimen in selected cases. Error bars indicate mean and s.d. values. Multiple group comparisons were made by ordinary one-way ANOVA test. During post hoc analyses, Dunnett's multiple comparisons test analyzed differences between the standard  $14 \pm 2$  days group with others in the maintenance pooled analyses in **a** and **b**, and patient (PT) untreated values with other groups in **b** and **e**, during the induction period, respectively. Adjusted  $P$  values for multiple testing are indicated. The  $P$  value comparing the controls versus untreated patients was 0.9795 in **e**. Number of samples investigated for each parameter: total C5, 19 healthy controls and 114 samples from 15 patients with CHAPLE disease; eculizumab concentrations, 96 samples from 15 patients; CH50, 14 healthy controls and 121 samples from 15 patients; AH50, 9 healthy controls and 25 samples from 13 patients.

healthy controls (AMCs) (Fig. 4 and Supplementary Fig. 7f,g). After treatment, free C5, C5a, sC5b–6 and sC5b–9 were swiftly reduced. Also, we found increased C4b and CFH but no reduction in C3a with therapy (Fig. 4b,e,f,g,k). Intriguingly, we detected a temporary increase in total C3 and inactive C3b, but not C3b, with treatment (Fig. 4c). Perhaps the active C3b is rapidly inactivated by the inhibitory proteins, including CFH and Factor I. These changes may be secondary to dissociation of the C5-convertase complexes (by regu-

lators other than CD55) upon abrupt removal of their substrate, the C5 molecule, from circulation since the eculizumab-bound form is inaccessible to the enzyme. Overall, eculizumab blocked the generation of the terminal complement activation mediators in patients with CHAPLE disease and caused secondary upstream effects.

C4 concentrations remained stable during treatment, but four subjects, P4, P5 and P7, with a history of thrombosis, and P6 with thrombocytosis, showed increased C4 (Fig. 4c). We evaluated C4

CNV and found two patients had two C4 copies, six with three C4 copies, one with four C4 copies and one with six C4 copies determined by estimation by WGS coverage (Supplementary Fig. 7h). The most common copy number of C4 genes, present between 50% and 60% of healthy human subjects, was four copies, but most of our patients had fewer C4 copies<sup>24,25</sup>. Interestingly, consistently high serum C4 values were found in P5 and P6, even after 6 months of treatment, and they had the highest C4 copy number among all patients we followed. High serum C3 and C4 are associated with venous thrombosis in postnatal women or in the context of individuals with antiphospholipid antibodies, suggesting that the correlation of thrombosis and high C4 concentrations due to CNV in our patients could be significant<sup>26,27</sup>. Our findings suggest that genetic variations in complement genes may account for disease expressivity or variable treatment responsiveness among different CD55-deficient individuals.

**Mutant soluble CD55 does not prevent complement hyperactivation.** The mutation in P12 inserted a stop codon for residue Gly348, which prevented addition of the glycerol phosphate-inositol membrane anchor and allowed CD55 to escape as a soluble serum form (Supplementary Fig. 9). Although typically membrane bound, CD55 is also secreted as a soluble form that inhibits complement in the fluid phase<sup>28</sup>. P12 was as sick as the other patients, suggesting that this mutant soluble version of CD55 was not protective in the context of GI disease.

**Microbiome changes following therapy.** Pathological alterations of the gut microbiota have been observed in inflammatory and metabolic diseases<sup>15</sup>. Specifically, reductions in alpha diversity and increases in abundance of *Enterobacteriaceae* taxa occur in chronic inflammatory conditions including inflammatory bowel disease, progressive human immunodeficiency virus infection and necrotizing enterocolitis<sup>29–33</sup>. We therefore performed metagenomic profiling of feces from six patients with CHAPLE disease before and after eculizumab. We observed a trend toward increased alpha diversity over 12 months of treatment ( $P=0.09$ , linear mixed-effects models, Fig. 5a). Pre- and post-treatment bacterial microbiota profiles clustered separately, and baseline microbiota profiles exhibited greater within-group dissimilarity (Fig. 5b,c). A similar profile was evident for fungi but not DNA viruses (Supplementary Fig. 10). Thus, eculizumab treatment causes microbiome restructuring toward a common gut microbial community, possibly by eliminating microbiome stressors, including inflammation, abnormal bowel movements, abnormal food intake and/or medications, including antibiotics. Moreover, the treatment decreased *Enterobacteriaceae* ( $P=0.013$ ,  $Q$  value (a  $P$  value that has been adjusted for the false discovery rate (FDR))=0.099, Fig. 5d)—pro-inflammatory gut pathogens associated with chronic inflammatory diseases<sup>34</sup>. Also, the

treatment increased *Bifidobacteriaceae* ( $P=0.012$ ,  $Q=0.096$ ) and *Faecalibacterium prausnitzii* ( $P=0.019$ ,  $Q=0.08$ ), which are important microbiota in healthy infants and are depleted in children with Crohn's disease (Fig. 5e,f)<sup>16,35</sup>. Thus, eculizumab treatment shifted the microbiota composition from an inflammatory profile to an enrichment of taxa comprising a healthy microbiome<sup>35</sup>.

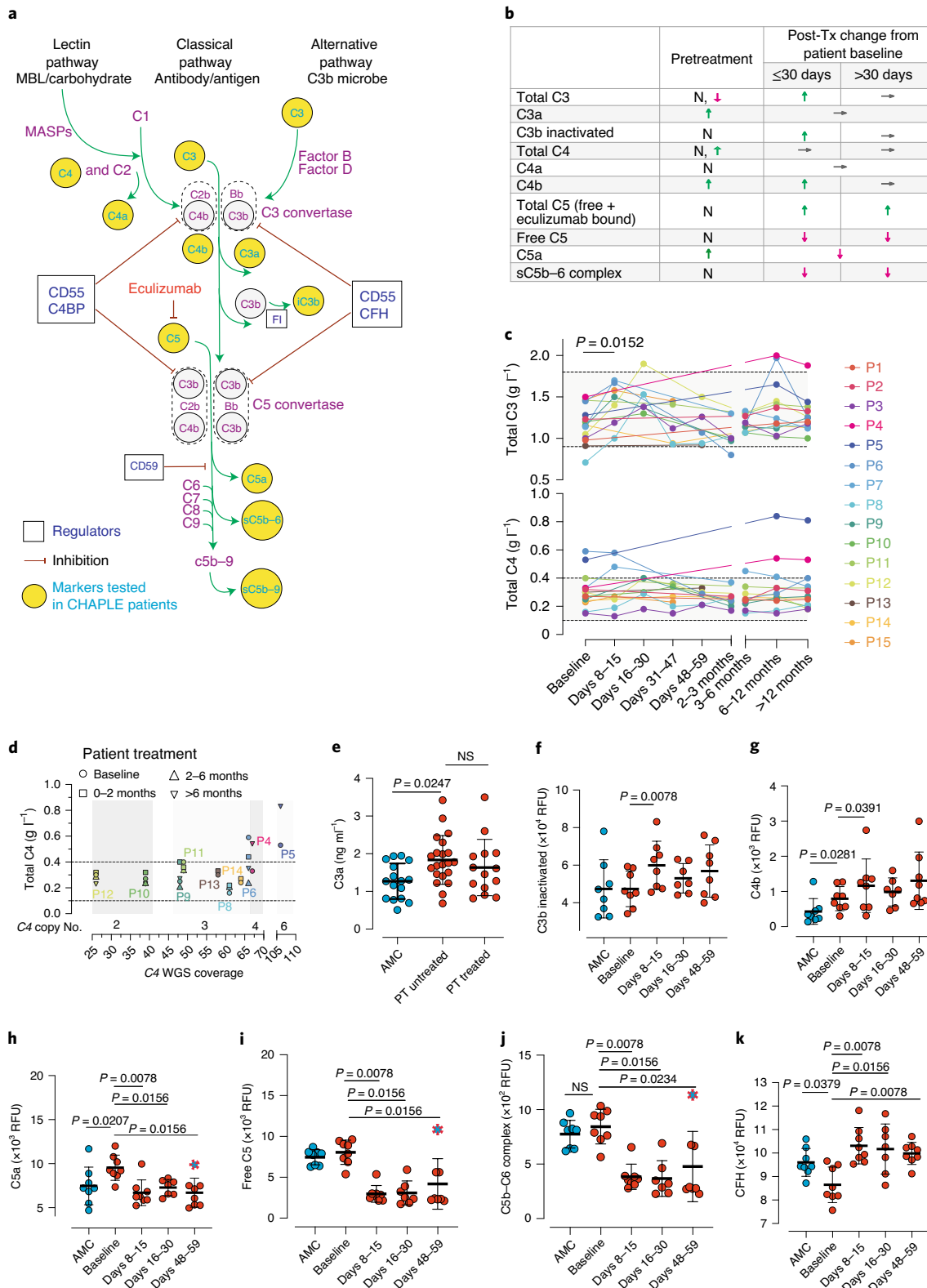
**Metabolic response to therapy.** To explore metabolic abnormalities, we profiled 1305 serum proteins in eight patients using the SOMALogic aptamer platform; 94 proteins differed significantly between patients and AMCs at baseline with  $Q < 0.05$  (Fig. 6a and Supplementary Fig. 11). Interestingly, despite PLE, only 26 proteins were reduced (Fig. 6a), whereas 68 proteins were increased (Fig. 6a). Of the 68 upregulated proteins, the greatest increases were in insulin-like growth factor (IGF) binding protein 2 (IGFBP2), REG4, ADSL, NACA, APOE, MMP3, PYY, GSK3A and GSK3B, CCL28 and PAPP. Of the 26 downregulated proteins, those with the greatest decreases were CA6, ADGRE2, BMP1, RET, CNTN4, APOM, NTRK3, EGFR, A2M and NTRK2, but CD55 was the lowest of any serum protein (Supplementary Fig. 12a,b). After eculizumab, the baseline patient values shifted closer to AMCs, especially for downregulated proteins (Supplementary Fig. 12c). At days 48–59, 23 of 26 downregulated proteins recovered (Fig. 6b and Supplementary Fig. 12d), but only 18 upregulated proteins were reduced (Fig. 6b and Supplementary Fig. 12d). In an unsupervised principal component analysis (PCA), patient samples at baseline (olive) moved progressively closer towards the controls (red) at 8–15 days (purple), 16–30 days (bright green) and, even more so, at 48–59 days (blue) (Fig. 6c). The PCA confirms that decreased proteins recover almost completely, whereas the increased proteins reversed but never to normal (Fig. 6c). To validate the SOMALogic protein changes, we used an enzyme-linked immunosorbent assay (ELISA) to check IGFBP2, which had the greatest elevation in disease and responded to therapy. The ELISA confirmed elevated IGFBP2 and its correction after treatment (Fig. 6d). Moreover, in P7 and P8, we found that a treatment delay caused an abrupt increase in IGFBP2, suggesting that it is a sensitive biomarker of disease activity.

We also observed that certain proteins normal at baseline in patients with CHAPLE disease changed after eculizumab therapy. In a rank analysis, soluble erythropoietin receptor (EPOR)—a protein involved in endothelial repair—showed the greatest increase (Fig. 6e,f)<sup>36,37</sup>. Among proteomic alterations, complement and coagulation pathways were the top-ranking functional groups, despite an  $FDR > 0.05$  (Extended Data Fig. 6a). CD55 regulates complement, innate immunity and coagulation, so we selected 53 complement and coagulation proteins measured by SOMALogic and determined that half (24/53) showed changes at baseline or following therapy (Supplementary Fig. 13).

**Fig. 4 | Blood concentrations of complement proteins and their activated products before and during eculizumab treatment.** **a**, Pathway schematic of the complement system. iC3b, inactivated C3b; FI, complement factor I; CFH, Complement factor H; MASP, mannose-associated serine protease. **b**, Summary of alterations in selected circulating complement markers in patients with CHAPLE disease. Arrows indicate the direction of change, if any: down arrow, decrease; up arrow, increase; or horizontal arrow, no change. N, normal. **c**, Blood concentration ( $\text{g l}^{-1}$ ) of intact C3 and C4 at baseline and during eculizumab treatment. Mean of repeated measurements at each time interval was plotted for individual patients. A mixed-effects model assessed the significance between values at different timepoints, with Tukey's multiple comparisons test calculating adjusted  $P$  values for each pair ( $n=15$  patients). **d**, Serum C4 levels in relation to estimated complement C4 gene copy numbers based on C4 WGS coverage. In **c** and **d**, horizontal dashed lines show reference ranges. **e**, Plasma C3a concentrations with respect to patient treatment status. **f–j**, Serial assessment of the serum complement components inactivated C3b (**f**), component C4b (**g**), anaphylatoxin C5a (**h**), free C5 (**i**) and soluble C5b–C6 complex (**j**). **k**, Soluble phase inhibitor CFH levels at baseline and during treatment. Statistics used to compare C3a between the three groups included an ordinary one-way ANOVA and Tukey's multiple comparisons test. Adjusted  $P$  values are indicated. Mann-Whitney (for comparing AMC versus patient baseline values) and Wilcoxon matched-pairs signed-rank tests (between patient baseline versus different post-treatment timepoints) analyzed the differences between groups in **f–k** ( $n=8$  control subjects and  $n=8$  patients for each analysis). Red dashed symbols filled with blue in **h–j** indicate values that correspond to dropped eculizumab concentrations after dose skipping. All  $P$  values are two-sided. Sample size for C3a: 16 AMC, 21 untreated patients and 13 treated patients. Error bars indicate mean and s.d. MBL, mannose-binding lectin; RFU, relative fluorescence units.

We also found substantial increases in proteins containing Ig-like domains (Supplementary Fig. 14). A tiny cluster (64 proteins) of such proteins were decreased (Extended Data Fig. 6b, blue lines). This cluster included several important immunoregulatory pro-

teins, especially cell adhesion molecules, and showed an impressive recovery with treatment (Extended Data Fig. 6b and Supplementary Fig. 15). Interestingly, 12 of the 27 immune-related molecules altered at baseline responded to eculizumab (Supplementary Fig.





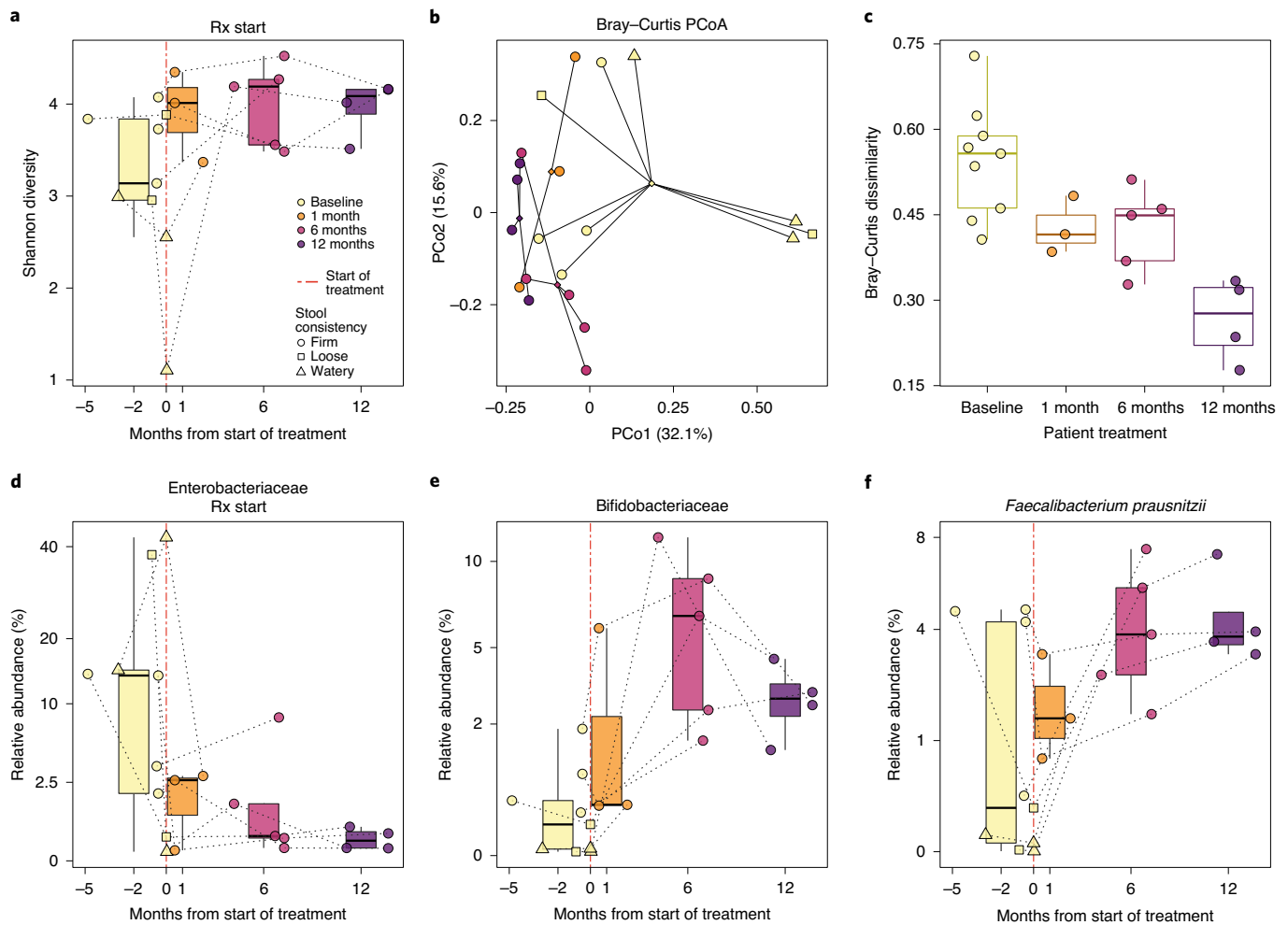


**Fig. 5 | Microbiota composition shifts in ecuzumab-treated patients with CHAPLE disease.** **a**, Shannon alpha diversity increases pre- and post-ecuzumab treatment are shown. Longitudinal samples from the same patient are connected by dotted lines. A statistical trend toward increased Shannon diversity is seen post-ecuzumab treatment (linear mixed-effects (LME) unadjusted  $P=0.09$ ). **b**, Principal coordinates analysis (PCoA) based on Bray-Curtis beta diversity metric of bacterial taxonomic abundances showing clustering by pre- and post-treatment timepoints (PERMANOVA  $P=0.03$ ). Centroids of community distances for each timepoint group are shown as diamonds. **c**, Bray-Curtis dispersions (scaled distance from centroid) within each timepoint group (analysis of variance (ANOVA)  $P=0.00066$ ). **d**, Enterobacteriaceae family abundances (LME  $P=0.013$ , FDR  $Q=0.099$ ). **e**, Bifidobacteriaceae family abundances (LME  $P=0.012$ ,  $Q=0.096$ ). **f**, *Faecalibacterium prausnitzii* species abundances (LME  $P=0.019$ ,  $Q=0.08$ ) across time in patients with CHAPLE disease. In **a** and **c-f**, the center bar denotes the median, the boxes denote interquartile range and the whiskers denote the interquartile range  $\times 1.5$ . The mean of multiple assessments is used for analysis if there is more than one measurement for an individual during a particular time period.  $n=6$  patients for all analyses.  $Q$  value is a  $P$  value that has been adjusted for the FDR. PCo1, principal coordinate 1; PCo2, principal coordinate 2.

16). Thus, inhibiting complement at the C5 level corrects many, but not all, immune and inflammatory abnormalities.

## Discussion

We studied the compassionate use of ecuzumab ‘off label’ to treat 16 CHAPLE cases with distinct *CD55* gene mutations. We were interested to understand how pharmacological inhibition downstream of C5 will affect immune dysregulatory disease caused by *CD55* loss by affecting upstream control at the C3 convertase. Previously, three members of a single family with CHAPLE disease improved with ecuzumab treatment<sup>3,13</sup>. This success, and the global emergence of more CHAPLE cases, posed key immunological and metabolic questions that we have now investigated. We demonstrate that ecuzumab is broadly effective in patients with CHAPLE disease with different *CD55* gene mutations. Recovery from complement damage to gut lymphatics was achieved rapidly in 100% of cases. The loss of immunoglobulins, infections and long-standing func-

tional GI abnormalities were substantially reversed, indicating that complement-mediated GI inflammation and lymphatic damage is reversible. However, the effects of the drug were temporary. We saw an immediate flare-up of symptoms and serum albumin and immunoglobulin loss when the medication was withdrawn. This observation implies that complement and its innate immune and inflammatory effector mechanisms are constantly stimulated, and that patients will require continuous treatment. Thus, ecuzumab effectively treats, but does not cure, CHAPLE disease. Nonetheless, despite the high cost of ecuzumab, our data support its early and continued use in CHAPLE disease. In addition, the therapeutic potential of an upstream blockade at the C3 level or combinatorial approaches with C3 and C5 blockade at different checkpoints could be considered in future studies, especially in patients with residual findings such as thrombocytosis or thrombosis.

We also explored dosing regimens because ecuzumab is extremely expensive, and insurance/health agencies are reluctant

to pay for off-label use. The previous study recommended an augmented induction regimen based on the theory that PLE would limit drug effectiveness, at least early during treatment<sup>3,13</sup>. However, we found that this was unnecessary. Our measurements of eculizumab, total C5 (C5+eculizumab), AH50 and CH50 showed that inhibitory blood concentrations were achieved rapidly, indicating that lymphatic leakage and PLE were surprisingly quickly mended. We also spaced out dosing intervals and found that almost half of

the patients required only 30-day maintenance doses, which substantially reduced the cost.

Serum proteomics revealed that GI disease and protein-wasting in patients with CHAPLE disease cause a starvation state, thereby explaining the physiological abnormalities in growth, activity and maturation. We found that the downregulated proteins were mostly rescued (23 of 26) by treatment, likely due to the prevention of lymph protein loss and anabolic processes. In intestinal lymphan-

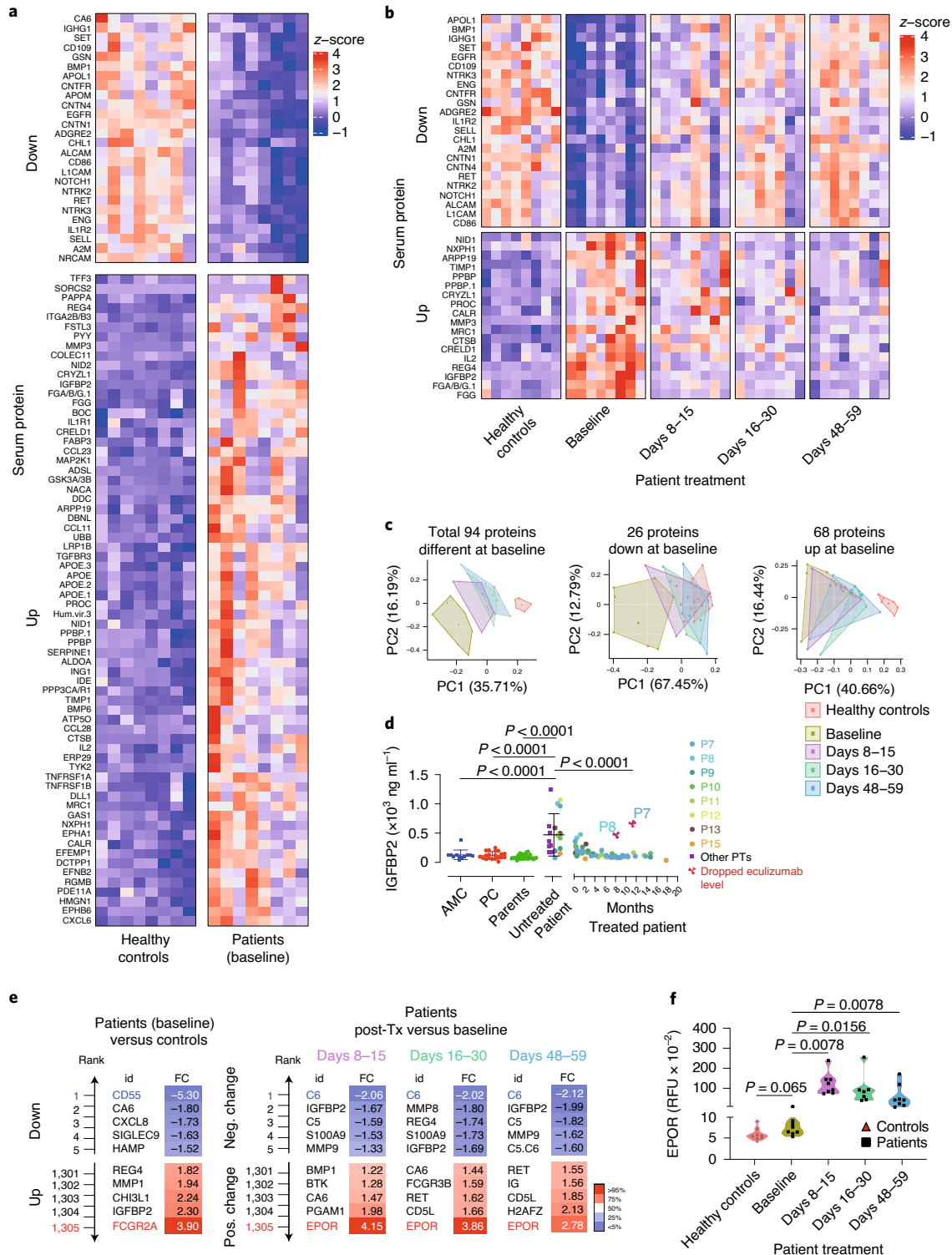


**Fig. 6 | Serum proteins altered in patients and response to eculizumab therapy.** **a**, Compared with healthy AMCs, patients at baseline showed 94 proteins with differences significant at  $P < 0.05$  (two-sided) after correcting for multiple testing of all 1305 proteins measured; 26 of these proteins were downregulated and 68 were upregulated in the patients. **b**, Comparing baseline to post-treatment timepoints for the patients up to day 59 showed 41 proteins with differences significant at  $P < 0.05$  (two-sided) after correcting for multiple testing of the 94 proteins analyzed due to a difference at baseline. All 41 proteins changed towards the level observed in healthy controls. **c**, PCA plots using all 94 proteins or, separately, those down- or upregulated in patients at baseline. **d**, Serum IGFBP2 concentrations. Statistics used an ordinary one-way ANOVA with Dunnett's multiple comparisons correction (numbers of samples: 12 AMC, 20 unrelated processing controls (PC), 36 parent samples, 20 samples from 14 untreated patients, 61 samples from 8 patients post-treatment). Error bars indicate mean and s.d. values. **e**, Top and bottom five proteins, ranked according to calculated  $\log_2(\text{FC})$  values, where FC means fold change, either in reference to controls (at baseline) or to pretreatment levels in the patients at the indicated timepoints (during eculizumab treatment). **f**, EPOR levels in RFU are shown. Comparison of healthy controls to baseline was made by Mann-Whitney test and inpatient comparisons by Wilcoxon matched-pairs signed-rank test (two-sided  $P$  value;  $n = 8$  patients and eight AMCs in **a-d** and **f**). The violin plots show the distribution of values across the minimum to maximum range. Protein measurements were performed on the SOMAlogic platform except for IGFBP2 in **d**, which was determined by ELISA. PC1, principal component 1; PC2, principal component 2; Pos., positive; Neg., negative.

giectasia, albumin and immunoglobulins are specifically lost<sup>38,39</sup>. We now show that immunoregulatory proteins with structural immunoglobulin domains are also selectively lost<sup>40</sup>. By contrast, only 18 of 68 upregulated proteins showed a significant correction with treatment. We conjecture that, because eculizumab blocks at the level of C5, immune activation and inflammation due to upstream C3a anaphylatoxin and C3b opsonization induces these proteins in a self-perpetuating process despite eculizumab therapy<sup>41</sup>. Interestingly, eculizumab treatment increased C3 and inactivated C3b. Similar changes occur in PNH following eculizumab, with erythrocytes accumulating C3d on their surface. Opsonized erythrocytes undergo extravascular hemolysis, reducing the treatment benefits<sup>42</sup>. Interestingly, total C4 concentration was elevated in patients with CHAPLE disease with four or six *C4* gene copies. We also found that a SNP encoding the V802I amino acid substitution in C5 protein alters the blood concentration of the eculizumab-bound C5 complex, with potential effects on alternative C5 activation through human neutrophil elastase<sup>17</sup>. Our data suggests that these genetic factors may modify disease activity and pharmacodynamic properties of eculizumab in CHAPLE disease.

Our proteomics revealed multiple coagulation factor abnormalities. Thus, CHAPLE disease involves the pathological cross-talk of complement abnormalities on coagulation similar to glycosylation disorders that also present with lymphangiectasia and coagulation abnormalities<sup>43</sup>. Further studies are needed to understand the intersection of complement and coagulation pathways, especially in unexplained lymphangiectasia disorders. Interestingly, we found IGFBP2 to be a sensitive biomarker. High IGFBP2 concentrations were reported in various kidney diseases<sup>44</sup>. It is highly expressed in different cancers and promotes angiogenesis by enhancing vascular endothelial growth factor (VEGF) expression<sup>45</sup>. We did not detect an apparent renal phenotype in CHAPLE; perhaps the biological IGFBP2 activity may be relevant to the circulatory features<sup>46</sup>. Unexpectedly, we found eculizumab treatment was also associated with increases in certain serum proteins that were normal in untreated disease. The EPOR showed the largest increase. Recent studies indicate that the EPOR is expressed in endothelial cells and is essential for healthy vasculature and vessel repair<sup>36,37</sup>. Thus, EPOR function may contribute to the therapeutic effects of eculizumab in healing damaged GI lymphatic vessels.

Genetic deficiencies of the complement inhibitors CD46, CD55 and CD59 reveal protective roles in different organs. Germline CD55 deficiency in CHAPLE disease, like atypical hemolytic uremic syndrome, causes abnormalities in coagulation, hematopoietic cells and endothelium, although it has a selective impact on the GI lymphatic vasculature. CD55 is upregulated by diverse stress or danger signals, suggesting that it has cytoprotective roles during inflammation, coagulation and angiogenesis<sup>47</sup>. The same set of stimuli may

not produce an identical response in CD46 or CD59, implying that the dominant inhibitor is context-dependent<sup>48</sup>. For example, CD59 is expressed by blood vascular endothelial cells but is absent in lymphatic endothelium<sup>49</sup>. PNH involves a somatic mutation in erythrocytes, so presumably CD55 and CD59 are intact in the gut and prevent GI manifestations<sup>9</sup>.

Gut microbiota may provide the constant stimulus to complement activation in CHAPLE disease. Our metagenomic profiling showed that patients with CHAPLE disease have pathological microbiota such as inflammation-associated *Enterobacteriaceae* and reduced Shannon diversity. These are signs of a diseased GI tract and might provide the impetus for ongoing local complement hyperactivation. We found greater interpatient dissimilarity of microbiota before treatment, and homogenization afterwards. This is consistent with the 'Anna Karenina' principle, whereby GI diseases cause distinct abnormal microbiota profiles in different patients, whereas microbiota configurations in healthy people converge toward a more homogeneous structure<sup>50</sup>. Eculizumab treatment removes microbiota stressors and rebalances a healthy microbiome.

### Online content

Any methods, additional references, Nature Research reporting summaries, source data, extended data, supplementary information, acknowledgements, peer review information; details of author contributions and competing interests; and statements of data and code availability are available at <https://doi.org/10.1038/s41590-020-00830-z>.

Received: 18 June 2020; Accepted: 28 October 2020;

Published online: 4 January 2021

### References

1. Waldmann, T. A., Steinfeld, J. L., Dutcher, T. F., Davidson, J. D. & Gordon, R. S. Jr. The role of the gastrointestinal system in 'idiopathic hypoproteinemia'. *Gastroenterology* **41**, 197–207 (1961).
2. Ozen, A. et al. CD55 deficiency, early-onset protein-losing enteropathy, and thrombosis. *N. Engl. J. Med.* **377**, 52–61 (2017).
3. Kurolap, A. et al. Loss of CD55 in eculizumab-responsive protein-losing enteropathy. *N. Engl. J. Med.* **377**, 87–89 (2017).
4. Ozen, A. CHAPLE syndrome uncovers the primary role of complement in a familial form of Waldmann's disease. *Immunol. Rev.* **287**, 20–32 (2019).
5. Mevorach, D. Clearance of dying cells and systemic lupus erythematosus: the role of C1q and the complement system. *Apoptosis* **15**, 1114–1123 (2010).
6. Holers, V. M. Complement and its receptors: new insights into human disease. *Annu. Rev. Immunol.* **32**, 433–459 (2014).
7. Kwan, W. H., van der Touw, W. & Heeger, P. S. Complement regulation of T cell immunity. *Immunol. Res.* **54**, 247–253 (2012).
8. Elvington, M., Liszewski, M. K. & Atkinson, J. P. Evolution of the complement system: from defense of the single cell to guardian of the intravascular space. *Immunol. Rev.* **274**, 9–15 (2016).

9. Zipfel, P. F. & Skerka, C. Complement regulators and inhibitory proteins. *Nat. Rev. Immunol.* **9**, 729–740 (2009).
10. Rother, R. P., Rollins, S. A., Mojcić, C. F., Brodsky, R. A. & Bell, L. Discovery and development of the complement inhibitor eculizumab for the treatment of paroxysmal nocturnal hemoglobinuria. *Nat. Biotechnol.* **25**, 1256–1264 (2007).
11. Wong, E. K., Goodship, T. H. & Kavanagh, D. Complement therapy in atypical haemolytic uraemic syndrome (aHUS). *Mol. Immunol.* **56**, 199–212 (2013).
12. Harris, C. L., Pouw, R. B., Kavanagh, D., Sun, R. & Ricklin, D. Developments in anti-complement therapy; from disease to clinical trial. *Mol. Immunol.* **102**, 89–119 (2018).
13. Kurolap, A. et al. Eculizumab is safe and effective as a long-term treatment for protein-losing enteropathy due to CD55 deficiency. *J. Pediatr. Gastroenterol. Nutr.* **68**, 325–333 (2019).
14. Di Narzo, A. F. et al. High-throughput identification of the plasma proteomic signature of inflammatory bowel disease. *J. Crohns Colitis* **13**, 462–471 (2019).
15. Pickard, J. M., Zeng, M. Y., Caruso, R. & Núñez, G. Gut microbiota: role in pathogen colonization, immune responses, and inflammatory disease. *Immunol. Rev.* **279**, 70–89 (2017).
16. Schwiertz, A. et al. Microbiota in Pediatric Inflammatory Bowel Disease. *J. Pediatr.* **157**, 240–244.e1 (2010).
17. Giles, J. L., Choy, E., van den Berg, C., Morgan, B. P. & Harris, C. L. Functional analysis of a complement polymorphism (rs17611) associated with rheumatoid arthritis. *J. Immunol.* **194**, 3029–3034 (2015).
18. Hillebrandt, S. et al. Complement factor 5 is a quantitative trait gene that modifies liver fibrogenesis in mice and humans. *Nat. Genet.* **37**, 835–843 (2005).
19. Schatz-Jakobsen, J. A. et al. Structural basis for eculizumab-mediated inhibition of the complement terminal pathway. *J. Immunol.* **197**, 337–344 (2016).
20. Fukuzawa, T. et al. Long lasting neutralization of C5 by SKY59, a novel recycling antibody, is a potential therapy for complement-mediated diseases. *Sci. Rep.* **7**, 1080 (2017).
21. Zelek, W. M., Taylor, P. R. & Morgan, B. P. Development and characterization of novel anti-C5 monoclonal antibodies capable of inhibiting complement in multiple species. *Immunology* **157**, 283–295 (2019).
22. Ardissino, G. et al. Complement functional tests for monitoring eculizumab treatment in patients with atypical hemolytic uremic syndrome: an update. *Pediatr. Nephrol.* **33**, 457–461 (2018).
23. Lintner, K. E. et al. Early components of the complement classical activation pathway in human systemic autoimmune diseases. *Front Immunol.* **7**, 36 (2016).
24. Yang, Y. et al. Gene copy-number variation and associated polymorphisms of complement component C4 in human systemic lupus erythematosus (SLE): low copy number is a risk factor for and high copy number is a protective factor against SLE susceptibility in European Americans. *Am. J. Hum. Genet.* **80**, 1037–1054 (2007).
25. Saxena, K. et al. Great genotypic and phenotypic diversities associated with copy-number variations of complement C4 and RP-C4-CYP21-TNX (RCCX) modules: a comparison of Asian-Indian and European American populations. *Mol. Immunol.* **46**, 1289–1303 (2009).
26. Dahm, A. E. A. et al. Elevated complement C3 and C4 levels are associated with postnatal pregnancy-related venous thrombosis. *Thromb. Haemost.* **119**, 1481–1488 (2019).
27. Savelli, S. L. et al. Opposite profiles of complement in antiphospholipid syndrome (APS) and systemic lupus erythematosus (SLE) among patients with antiphospholipid antibodies (aPL). *Front Immunol.* **10**, 885 (2019).
28. Medof, M. E., Walter, E. I., Rutgers, J. L., Knowles, D. M. & Nussenzweig, V. Identification of the complement decay-accelerating factor (DAF) on epithelium and glandular cells and in body fluids. *J. Exp. Med.* **165**, 848–864 (1987).
29. Kostic, A. D. et al. Genomic analysis identifies association of *Fusobacterium* with colorectal carcinoma. *Genome Res* **22**, 292–298 (2012).
30. Arthur, J. C. et al. Intestinal inflammation targets cancer-inducing activity of the microbiota. *Science* **338**, 120–123 (2012).
31. Lloyd-Price, J. et al. Multi-omics of the gut microbial ecosystem in inflammatory bowel diseases. *Nature* **569**, 655–662 (2019).
32. Vujkovic-Cvijin, I. et al. Dysbiosis of the gut microbiota is associated with HIV disease progression and tryptophan catabolism. *Sci. Transl. Med.* **5**, 193ra191 (2013).
33. Olm, M. R. et al. Necrotizing enterocolitis is preceded by increased gut bacterial replication, *Klebsiella*, and fimbriae-encoding bacteria. *Sci. Adv.* **5**, eaax5727 (2019).
34. Shin, N. R., Whon, T. W. & Bae, J. W. Proteobacteria: microbial signature of dysbiosis in gut microbiota. *Trends Biotechnol.* **33**, 496–503 (2015).
35. Blanton, L. V. et al. Gut bacteria that prevent growth impairments transmitted by microbiota from malnourished children. *Science* **351**, aad3311 (2016).
36. Heeschen, C. et al. Erythropoietin is a potent physiologic stimulus for endothelial progenitor cell mobilization. *Blood* **102**, 1340–1346 (2003).
37. Ribatti, D. et al. Human erythropoietin induces a pro-angiogenic phenotype in cultured endothelial cells and stimulates neovascularization in vivo. *Blood* **93**, 2627–2636 (1999).
38. Homburger, F. & Petermann, M. L. Studies on hypoproteinemia; familial idiopathic dysproteinemia. *Blood* **4**, 1085–1108 (1949).
39. Parfitt, A. M. Familial neonatal hypoproteinaemia with exudative enteropathy and intestinal lymphangiectasis. *Arch. Dis. Child* **41**, 54–62 (1966).
40. Srinivasan, M. & Roeske, R. W. Immunomodulatory peptides from IgSF proteins: a review. *Curr. Protein Pept. Sci.* **6**, 185–196 (2005).
41. Sauter, R. J. et al. Functional relevance of the anaphylatoxin receptor C3aR for platelet function and arterial thrombus formation marks an intersection point between innate immunity and thrombosis. *Circulation* **138**, 1720–1735 (2018).
42. Notaro, R. & Sica, M. C3-mediated extravascular hemolysis in PNH on eculizumab: mechanism and clinical implications. *Semin Hematol.* **55**, 130–135 (2018).
43. Brucker, W. J. et al. An emerging role for endothelial barrier support therapy for congenital disorders of glycosylation. *J. Inher. Metab. Dis.* **43**, 880–890 (2020).
44. Ding, H., Kharboutli, M., Saxena, R. & Wu, T. Insulin-like growth factor binding protein-2 as a novel biomarker for disease activity and renal pathology changes in lupus nephritis. *Clin. Exp. Immunol.* **184**, 11–18 (2016).
45. Azar, W. J. et al. IGFBP-2 enhances VEGF gene promoter activity and consequent promotion of angiogenesis by neuroblastoma cells. *Endocrinology* **152**, 3332–3342 (2011).
46. Ozen, A., Comrie, W. A. & Lenardo, M. J. CD55 deficiency and protein-losing enteropathy. *N. Engl. J. Med.* **377**, 1499–1500 (2017).
47. Mason, J. C., Lidington, E. A., Ahmad, S. R. & Haskard, D. O. bFGF and VEGF synergistically enhance endothelial cytoprotection via decay-accelerating factor induction. *Am. J. Physiol. Cell Physiol.* **282**, C578–C587 (2002).
48. Mason, J. C. et al. Induction of decay-accelerating factor by cytokines or the membrane-attack complex protects vascular endothelial cells against complement deposition. *Blood* **94**, 1673–1682 (1999).
49. Park, S. M. et al. Mapping the distinctive populations of lymphatic endothelial cells in different zones of human lymph nodes. *PLoS ONE* **9**, e94781 (2014).
50. Zaneveld, J. R., McMinds, R. & Vega Thurber, R. Stress and stability: applying the Anna Karenina principle to animal microbiomes. *Nat. Microbiol.* **2**, 17121 (2017).

**Publisher's note** Springer Nature remains neutral with regard to jurisdictional claims in published maps and institutional affiliations.

© The Author(s), under exclusive licence to Springer Nature America, Inc. 2021

## Methods

**Clinical study information.** This manuscript reports an observational clinical study reporting on the outcome of eculizumab therapy in patients with CHAPLE disease treated in a noninterventional setting in which we collected data on exploratory biomedical parameters. Institutional review board approval was obtained from the Marmara University Medical Faculty Institutional Review Board for Clinical Research. We recruited verified patients with CD55 deficiency who were assigned by their physicians to receive eculizumab for enrollment in this study. All patients, or their parents for minor subjects, provided written informed consent for the study in accordance with the Declaration of Helsinki. Exclusion criteria included: (1) presence of a concomitant disease that leads to hypoproteinemia at the time of starting eculizumab, (2) presence of a concomitant disease that leads to secondary intestinal lymphangiectasia and (3) unstable clinical condition that precludes drawing blood (for biomarker studies). A total of 15 patients enrolled in the study through Marmara University and all are reported on in this manuscript. P16 was treated in the Netherlands and included in the analyses. We collected clinical data to assess: (1) reversal of PLE; (2) reversal of patient-specific major symptoms; (3) reversal of other systemic components of the disease; (4) correction of previous biochemical and radiological abnormalities; and (5) cessation of previous medications.

**Dosing regimen.** Patients were given an infusion of the complement C5 blocker eculizumab under the brand name Soliris according to the following dosing regimen. Patients older than 18 years of age were given 900 mg weekly for the first 4 weeks and maintained with 1,200 mg every other week. For patients younger than 18 years of age, eculizumab was administered on a weight-dependent schedule as shown in in Supplementary Table 1. Eculizumab was administered within 2 days of the recommended dosage regimen timepoint. Three patients (P14, P15 and P16) received a modified regimen during the induction phase as proposed by Kurolop et al.<sup>13</sup>: first, four eculizumab doses given as two injections per week for two consecutive weeks (treatment days 1, 4, 8 and 11), followed by three weekly doses (treatment days 15, 22 and 29); thereafter, maintenance infusions on a biweekly basis.

**Clinical markers.** Clinical measurements of patient serum were taken at baseline and before each infusion. Total protein, albumin and IgG, IgM, IgA and IgE were measured alongside complete blood counts and the safety laboratory tests. Additional analyses included the coagulation markers activated partial thromboplastin time, D-dimer and fibrinogen; the additional safety markers total and direct bilirubin, the complement proteins C3, C4, C5 and CH50; and the malabsorption parameters vitamins B12 and D, folate, ferritin, iron, iron binding capacity, calcium, magnesium and blood lipids.

**Symptom diaries.** We collected self-reported daily symptom diaries that tracked abdominal pain, nausea, vomiting, bowel movements, stool formation, facial edema and inability to feed. Each symptom was scored and recorded daily according to scales described in Supplementary Fig. 5. The patients (adolescent and adults) or parents on behalf children (or youngsters) were asked to complete symptom diaries on daily basis. Data collection was started during the screening visit when patients were evaluated for eligibility for the study and only if a decision to initiate eculizumab was made. Prospectively collected symptom diaries were returned to their physicians on a monthly basis. Patient-reported symptom diaries were collected throughout the induction phase (4 weeks) plus the subsequent 10 weeks during maintenance; some patients continued filling the diaries for longer. Symptom scores were entered into a spreadsheet by the primary physician or the principal investigator and analyzed.

**QOL assessment.** The Turkish version 'KINDL' questionnaire was used to assess changes in QOL over the course of the trial, as was previously done (<https://www.kindl.org/english/language-versions/turkish/>)<sup>31</sup>. The questionnaire consists of 24 Likert-scaled items grouped into six subscales measuring specific aspects of QOL, including physical well-being, emotional well-being, self-esteem, family, friends and school. An additional 'Disease' module for patient's self-identifying as hospitalized or having a long-term illness was used. The presence of the symptom is evaluated based on a quintile Likert scale; 'never', 'rarely', 'sometimes', 'frequently' and 'always' options are scored by '1', '2', '3', '4' and '5', respectively. Subscale scores are produced by combining the item ratings for each of the six subscales and converting each subscale score to a scale of 0 to 100, with higher scores representing better QOL. Similarly, a total score is produced by combining the item ratings across all six subscales (not including the Disease module). The SPSS syntax files provided by the KINDL-R site were used to enter and analyze the KINDL-R data using the IBM SPSS Statistics trial version software package for MAC OS. The KINDL parent form was used for children aged 8–16 years old.

**Cells.** Peripheral blood mononuclear cells (PBMCs) were isolated from blood by Ficoll gradient density centrifugation. In short, blood was diluted 1:1 in phosphate buffered saline (PBS, Quality Biological). One volume of diluted blood was added to one volume of Ficoll-Paque PLUS density gradient media (GE Healthcare) and centrifuged at 1,200 r.p.m. for 20 min with the brakes off. PBMCs were isolated

from the interface of Ficoll and plasma and underwent ACK lysis (Quality Biological) to remove erythrocytes. PBMCs were aliquoted and cryopreserved in liquid nitrogen in fetal bovine serum containing 10% dimethyl sulfoxide.

**Flow cytometry.** PBMCs were incubated with human Fc receptor blocking solution (BioLegend) in PBS at 25 °C for 15 min. Cells were stained in ice cold fluorescence-activated cell sorting (FACS) buffer (PBS with 2% fetal calf serum and 1% sodium azide) with the following antibodies on ice for 30 min at specified dilutions: purified mouse allophycocyanin-conjugated anti-human CD3 antibody (BD, catalog no. 347340, clone SK7, dilution 1:10), purified mouse peridinin chlorophyll protein complex-conjugated anti-human CD19 antibody (BD, catalog no. 347540, clone 4G7, dilution 1:10) and purified mouse phycoerythrin-conjugated anti-human CD55 antibody (BioLegend, catalog no. 311302, clone JS11, dilution 1:100). Cells were washed in FACS buffer before acquisition on FACS Calibur (Becton Dickinson) and analyzed with FlowJo v.X (Becton Dickinson). Anaphylatoxins were measured using a Cytometric Bead Array Human Anaphylatoxin Kit (Becton Dickinson, catalog no. 561418). Analyses were performed on a Navios EX flow cytometer (Beckman Coulter). Gating strategy is summarized in Supplementary Fig. 1.

**Eculizumab and C5 concentrations.** Eculizumab concentrations were measured in serum samples using a liquid chromatography–tandem mass spectrometry (LC–MS/MS) method developed in house on a triple-quadrupole mass spectrometer under selected reaction monitoring (SRM) mode, referred to as SRM–LC–MS/MS. Briefly, total protein in serum samples is first denatured, reduced and digested with trypsin. The digested peptide mixtures are then analyzed by the SRM–LC–MS/MS method. Signature peptide(s) unique to eculizumab detected in the sample digests are monitored and quantitated using an eculizumab protein calibration curve. The lower limit of quantitation of the assay is 4 µg ml<sup>-1</sup>. Total C5 concentrations in human serum were measured in house using an electrochemiluminescence immunoassay that measures the concentration of total C5. Briefly, serum samples were diluted in mild acetic acid containing a biotinylated human anti-C5 antibody as capture reagent, then added into a streptavidin coated MesoScale Discovery plate. The C5 capture in the plate is then detected by a second ruthenium labeled anti-C5 antibody and quantified by a purified human C5 calibration curve. Lower limit of quantitation of the assay was 7.8 µg ml<sup>-1</sup>.

**Complement activity.** The CH50 assay tests the functional capability of complement components of the classical pathway using sheep red blood cells (SRBCs) pre-coated with rabbit anti-SRBC antibody. Briefly, each serum sample is serially diluted, and a fixed volume of optimally sensitized SRBCs is added to each diluted sample. After incubation, the mixture is centrifuged, and the degree of hemolysis is quantified by measuring the absorbance of the hemoglobin released into the supernatant at 415 nm. The dilution of patient's serum needed to lyse 50% of erythrocytes is then determined as the CH50 value. Similarly, the AH50 assay tests the functional capability of complement components of the alternative pathway using rabbit erythrocytes. A buffer containing EGTA is used to chelate calcium and block the activation of the classical pathway<sup>52</sup>.

**Fecal microbiome metagenomics.** DNA was isolated using the MagAttract PowerMicrobiome DNA/RNA EP Kit (Qiagen) in an Eppendorf epMotion 5073 automated liquid handling system. Metagenomic libraries were prepared using 30 µl of DNA in a 96-well plate with the Nextera DNA Flex Library Prep Kit (Illumina). Library preparation was initiated with tagmentation and post-tagmentation cleanup followed by amplification of tagmented DNA and cleanup using Sample Purification Beads for both the cleanup steps. Library quality control included quantification of the final library using the Qubit dsDNA High Sensitivity assay and library quality assessment using the Agilent High Sensitivity HS D5000 ScreenTape assay on the Agilent 4200 TapeStation. The individual libraries were diluted and pooled at a concentration of 7 nM to make the final library pool. This pool was normalized to 1.8 pM, spiked-in with 1% PhiX sequencing control and sequenced on an Illumina NextSeq 500 instrument.

**Microbiome analysis.** For sequence analysis, read pairs were trimmed for quality and adapter sequences using BBduk (<https://jgi.doe.gov/data-and-tools/bbttools/>). The pairs were subsequently assembled with the metaSPAdes pipeline from SPAdes<sup>53</sup>. Taxonomic assignment was done with Kraken2 using Bracken 2.5 for abundance estimation and the maxikraken2 (v\_1903\_140GB) database<sup>54</sup>. Sequences matching to the human genome were excluded from all analyses. Functional annotation of the metagenomes was done using Prodigal for computational gene finding, InterProScan 5 for annotation, the KEGG orthology for pathway assignment and MinPath for pathway abundance inference<sup>55–57</sup>. Differential abundance statistics were performed using MaAsLin2 (<https://huttenhower.sph.harvard.edu/maaslin/>) with arc-sin transformation and a linear mixed-effects model testing the difference in abundances over time per subject. Alpha diversity and ordination were computed with the vegan Community Ecology R package using the diversity and betadisper functions. Statistical analyses were performed with vegan's adonis and the lmerTest R package<sup>58</sup>.

**Serum.** Blood was collected in vacutainer tubes without coagulants. The tube was left undisturbed for 30 min after removal of the cap to allow the blood to clot. The tube was then spun at 1,000 r.p.m. for 10 min. Serum is the supernatant and was stored at  $-80^{\circ}\text{C}$  for later use in laboratory experiments.

**Plasma.** Blood was collected in acid citrate dextrose tubes to isolate PBMCs and plasma. After Ficoll gradient density centrifugation, plasma samples were collected and stored in an ultra-low temperature freezer for later use.

**Serum proteomics.** Serum proteomic analysis was performed using the aptamer-based SOMAscan 1.3k Assay (SomaLogic). SomaLogic detects 1,305 protein analytes and is optimized for analysis of human serum<sup>59</sup>. Briefly, aptamers are short single-stranded DNA sequences modified to confer specific binding to target proteins and can be highly multiplexed for discovery of biomarker signatures. The proteins quantified include cytokines, hormones, growth factors, receptors, kinases, proteases, protease inhibitors and structural proteins. A complete list of the analytes measured is at <http://somalogic.com/wp-content/uploads/2017/06/SSM-045-Rev-2-SOMAscan-Assay-1.3k-Content.pdf>. The assay was performed according to manufacturer specifications and analyzed using web tools as previously described<sup>60,61</sup>.

**Complement markers.** Serum C3 and C4 concentrations were determined in the clinical laboratory on fresh blood samples using a turbidimetric method.

Plasma anaphylatoxins (C3a, C4a and C5a) were measured using a flow cytometry based Cytometric Bead Array Human Anaphylatoxin Kit.

The sC5b-9 levels were measured using MicroVue sC5b-9 Plus EIA kit (Quidel Corporation) according to the manufacturer's protocol and as reported elsewhere<sup>62</sup>. The plasma samples were diluted to 1:10 using the sample diluent provided with the kit. The sC5b-9 was detected by the detection antibody (horseradish peroxidase-conjugated anti-sC5b-9 complex). The signal was developed by adding a chromogenic enzyme-substrate and measured using a spectrophotometer.

Free C5, C3b, inactivated C3b, C4b and soluble C5b-6 complex (sC5b-6) assessments were made by the SOMAlogic platform using biobanked serum samples as described elsewhere<sup>63</sup>. To test for the active and inactive forms of C3b, the SOMAmers 2683-1 and 4480-59 were used. Per the manufacturer's specifications, SOMAmer 2683-1 was selected against iC3b isolated from human serum, with a similar binding to C3 and C3b. SOMAmer 4480-59 was selected against C3b isolated from human serum; a binding to C3 and iC3b was observed, but it was at least 10 $\times$  weaker affinity. There was no binding with the C3d or C3a fragments. The characterization of the SOMAmers is presented Supplementary Table 2.

**IGFBP2 measurement in serum samples.** IGFBP2 concentration was measured in serum samples using a DuoSet ELISA kit (R&D Systems, catalog no. DY674) according to the manufacturer's protocol and as described elsewhere<sup>64</sup>. Briefly, the 96-well microplates were coated with the capture antibody (mouse anti-human IGFBP2) overnight at  $25^{\circ}\text{C}$ . The serum samples were diluted to 1:250 using the assay buffer provided with the kit. The standards or samples were loaded onto the microplate in duplicates and incubated for 2 h at  $25^{\circ}\text{C}$ . IGFBP2 was detected by the detection antibody (biotinylated goat anti-human IGFBP2) and streptavidin-horseradish peroxidase conjugate.

**Whole-genome sequencing.** Genomic DNA samples were quantified using a fluorescence dye-based assay (PicoGreen dsDNA reagent) before normalization to 20 ng  $\mu\text{l}^{-1}$  and 55  $\mu\text{l}$  of volume. Samples were added into a Covaris 96 microTUBE plate at 1,000 ng gDNA input and sheared using the Covaris LE220 Focused-ultrasonicator targeting a peak size of 410 bp. Sequencing libraries were generated from fragmented DNA using the Illumina TruSeq DNA PCR-Free HT Library Preparation Kit and IDT for Illumina TruSeq DNA UD Indexes (96 indexes, 96 samples) adapters with minor modifications for automation (Hamilton STAR Liquid Handling System). Library size distribution and absence of adapter dimers was assessed by automated capillary gel-electrophoresis (Advanced Analytical Fragment Analyzer). Library yield was determined by qPCR quantitation using the KAPA qPCR Quantification Kit (Roche Light Cycler 480 Instrument II). Sequencing libraries were normalized, pooled into a 24-plex and quantified as above before dilution to 2.7 nM and sequenced on an Illumina NovaSeq 6000 using a S4 Reagent Kit (300 cycles) using 151 + 8 + 8 + 151 cycle run parameters. Primary sequencing data was demultiplexed (demuxed) using the Illumina HAS2.2 pipeline and sample-level quality control for base quality, coverage, duplicates and contamination was conducted. The sequenced DNA reads were then mapped to hg19 or hg38 human genome reference using the Burrows-Wheeler Aligner with default parameters. Variant calling was performed using the Genome Analysis Toolkit v.3.4 (the Broad Institute, <http://www.broadinstitute.org/gatk/>).

For Complement C4 gene copy number, the coverage of the whole C4 regions, the unique C4 long form regions and control regions without CNV changes were calculated by bedtools after removing the duplicated reads and low-quality mapping reads. The coverage of C4 regions were then normalized by the control regions coverage and the rough copy number of C4 genes was estimated for diploid

genomes. The C4 long form copy numbers were determined by the coverage of the unique C4 intronic region in the C4 long form.

**Structural modeling of complement C5 and eculizumab interactions.** To model the interactions and variant impacts of complement C5 and eculizumab, complement C5 protein complexed with eculizumab heavy chain variable domains (PDB ID 515K) was loaded into protein modeling software package ChimeraX<sup>19,65,66</sup>. Variant V802I was created using the rotamerization component in ChimeraX, and associated intermolecular and intramolecular steric hindrances (clashes) were calculated based on the predominant rotamer predicted by the software.

**Statistics.** Unless otherwise stated, all statistical analysis was conducted in Prism (GraphPad) v.8.2.1 with a  $P$  value  $<0.05$  was considered significant. Statistical analysis was conducted to assess patients' responses to eculizumab therapy over several different lengths of treatment, as specified in the text. Kaplan-Meier curves were fitted to show cumulative frequency of various parameters as a function of age. To compare patients' serum albumin, total protein, serum immunoglobulins, total C3 and C4 concentrations and serum IgG a mixed-effects model with Tukey's multiple comparisons correction was used. We compared plasma C3a values between the three groups using an ordinary one-way ANOVA and Tukey's multiple comparisons test. Between group comparisons for plasma C5a and sC5b-9 were made by the Mann-Whitney test. The Wilcoxon matched-pairs signed-rank test was used to assess changes in KINDL QOL and platelet counts. Changes in symptom frequency were analyzed using the Friedman test with Dunn's multiple comparisons correction. Changes in blood triglycerides were assessed using a mixed-effects model with Dunnett's multiple comparisons correction. An ordinary one-way ANOVA with Dunnett's multiple comparisons correction was used to analyze levels of eculizumab, total C5 (free + eculizumab bound) and CH50 and IGFBP2 levels. Mann-Whitney test and Wilcoxon matched-pairs signed-rank test compared free C5, inactivated C3b, C4b, the soluble C5b-6 complex, CFH and EPOR levels. The statistics used for the Microbiome changes following therapy section are described in the Microbiome analysis section. For the proteomic analyses, changes in proteins between patients and AMC were evaluated by Mann-Whitney  $U$ -test, and longitudinal changes within patient by Wilcoxon signed-rank paired test, with  $P$  values corrected for multiple comparison by Benjamini-Hochberg method. There was no blinding in the clinical data acquisition as this is not a placebo-controlled trial. The researchers who carried pharmacokinetic and pharmacodynamic examinations were blinded to the study subjects since each tube containing a patient sample was labeled with a code that included no reference to treatment status of the subject. For the proteomic and metagenomic studies the technicians who analyzed the samples were blinded to the group allocation information. The bioinformaticians carried the computational analyses by matching the sample metadata with the experimental test results, each provided by independent researchers. The bioinformatician who analyzed WGS data was blinded to serum C4 values when calculating estimated C4 gene copy numbers, but not blinded to patient allocation when searching for C5 gene variants, since the latter analysis required appropriate filtering strategies.

**Reporting Summary.** Further information on research design is available in the Nature Research Reporting Summary linked to this article.

## Data availability

The microbiome sequencing data is linked to the National Center for Biotechnology Information (NCBI) BioProject ID [PRJNA629392](https://www.ncbi.nlm.nih.gov/bioproject/PRJNA629392). The raw data, including the adad file used to generate proteomic analyses, the data analysis codes used for microbiome analyses and all other data that support the findings of this study, are available from the corresponding authors upon request to the extent allowed by all laws and institutional policies regarding confidentiality of patient clinical information. The following datasets were used in the study: Peditools; string db; maxikraken2 (v\_1903\_140GB) database; gnomAD v.2.1.1; and 1000genome.

## References

- Eser, E. et al. The psychometric properties of the new Turkish generic health-related quality of life questionnaire for children (Kid-KINDL). *Turk Psikiyatri Derg* **19**, 409–417 (2008).
- Jaskowski, T. D., Martins, T. B., Litwin, C. M. & Hill, H. R. Comparison of three different methods for measuring classical pathway complement activity. *Clin. Diagn. Lab. Immunol.* **6**, 137–139 (1999).
- Bankevich, A. et al. SPAdes: a new genome assembly algorithm and its applications to single-cell sequencing. *J. Comput. Biol.* **19**, 455–477 (2012).
- Wood, D. E., Lu, J. & Langmead, B. Improved metagenomic analysis with Kraken 2. *Genome Biol.* **20**, 257 (2019).
- Ye, Y. & Doak, T. G. A parsimony approach to biological pathway reconstruction/inference for genomes and metagenomes. *PLoS Comput. Biol.* **5**, e1000465 (2009).

56. Kanehisa, M., Sato, Y., Furumichi, M., Morishima, K. & Tanabe, M. New approach for understanding genome variations in KEGG. *Nucleic Acids Res.* **47**, D590–D595 (2019).
57. Hyatt, D. et al. Prodigal: prokaryotic gene recognition and translation initiation site identification. *BMC Bioinform.* **11**, 119 (2010).
58. Kuznetsova, A., Brockhoff, P. & Christensen, R. lmerTest Package: tests in linear mixed effects models. *J. Stat. Softw.* <https://doi.org/10.18637/jss.v082.i13> (2017).
59. Gold, L. et al. Aptamer-based multiplexed proteomic technology for biomarker discovery. *PLoS ONE* **5**, e15004 (2010).
60. Candia, J. et al. Assessment of variability in the SOMAscan assay. *Sci. Rep.* **7**, 14248 (2017).
61. Cheung, F. et al. Web tool for navigating and plotting SomaLogic ADAT files. *J. Open Res. Softw.* **5**, 20 (2017).
62. Noris, M. et al. Dynamics of complement activation in aHUS and how to monitor eculizumab therapy. *Blood* **124**, 1715–1726 (2014).
63. Emilsson, V. et al. Co-regulatory networks of human serum proteins link genetics to disease. *Science* **361**, 769–773 (2018).
64. Eiseaman, J. L. et al. Evaluation of plasma insulin-like growth factor binding protein 2 and Her-2 extracellular domain as biomarkers for 17-allylamino-17-demethoxygeldanamycin treatment of adult patients with advanced solid tumors. *Clin. Cancer Res.* **13**, 2121–2127 (2007).
65. Goddard, T. D. et al. UCSF ChimeraX: meeting modern challenges in visualization and analysis. *Protein Sci.* **27**, 14–25 (2018).
66. Shapovalov, M. V. & Dunbrack, R. L. Jr. A smoothed backbone-dependent rotamer library for proteins derived from adaptive kernel density estimates and regressions. *Structure* **19**, 844–858 (2011).
67. Tezcan, I., Berkel, A. I., Ersoy, F. & Sanal, O. Sağlıklı Türk çocukları ve erişkinlerde turbidometrik yöntemle bakılan serum immunoglobulin düzeyleri. *Çocuk Sağlığı ve Hastalıkları Derg.* **32**, 649–656 (1996).
68. Slenter, D. N. et al. WikiPathways: a multifaceted pathway database bridging metabolomics to other omics research. *Nucleic Acids Res.* **46**, D661–D667 (2017).
69. Subramanian, A. et al. Gene set enrichment analysis: a knowledge-based approach for interpreting genome-wide expression profiles. *Proc. Natl Acad. Sci. USA* **102**, 15545–15550 (2005).
70. Szklarczyk, D. et al. STRING v11: protein–protein association networks with increased coverage, supporting functional discovery in genome-wide experimental datasets. *Nucleic Acids Res.* **47**, D607–D613 (2019).

## Acknowledgements

This work was supported in part by the Division of Intramural Research, National Institute of Allergy and Infectious Diseases, NIH, BCBB Support Services Contract HHSN316201300006W/HHSN27200002, and The Marmara University, Scientific Research Projects Committee (BAPKO, grant no. SAG-C-TUP-230119-0018). We thank the Turkish National Society of Allergy and Clinical Immunology (TNSACI)

for supporting travel expenses for the screening studies. We thank C. Kemper of the National Heart, Lung and Blood Institute for thoughtful editing of the final manuscript. We thank M. Quiñones, the Center for Human Immunology and the NIAID Microbiome Program, NIAID, NIH, for research support. We also thank A. Kiykim for patient care, A. Dalga and I. Tatli for technical assistance and H. Su and X. He for advice and assistance; D. Comrie, S. Kubo and J. Ravell for critical reading of the manuscript; and R. Kissinger for artwork. We thank important colleagues at Regeneron: A. N. Thomas for sample processing; C. Huang for biomarker analysis; H. Qiu, and E. Sook Yen for eculizumab analysis; and C. H. Lai, L. DeStefano and K. Donohue for total C5 analysis. Molecular graphics and analyses were performed with UCSF ChimeraX, developed by the Resource for Biocomputing, Visualization and Informatics at the University of California, San Francisco, with support from NIH R01-GM129325 and the Office of Cyber Infrastructure and Computational Biology, NIAID.

## Author contributions

A.O. and M.J.L. designed the trial and supervised all activities. A.O., M.J.L., I.V.-C., R. Apps, F.C., M.-D.W. and P.S. analyzed and interpreted data. O.H., J.T. and Y.B. supervised activities and interpreted data. R. Apps, G.F., B.S., Y.G.N., K.D.-N. and G.A. conducted experiments. Y.Z., A.L.S., C.L., C.A. and C.L.D. performed genetic sequencing and data analyses. A.O., S.B., E.K.-A., S.B.E., N.K., M.S., E. Tutar, D.E., B.A., S.S., F.O., D.K.U., A.I., O.B.S., G.K., E. Topal, E.S., R.H.J.H., S.N.G., A.B., I.O. and B.D. provided patient care and collected data. D.E., E. Tutar, R. Artan and B.A. conducted gastrointestinal interventions. C.C. made histopathology evaluations. R.E. provided radiological assessment. A.O., S.D.C. and M.J.L. wrote the paper. All authors reviewed, edited and approved the manuscript.

## Competing interests

The authors M.J.L. and A.O. have a pending patent on C5 inhibitor treatment of CHAPLE. B.S. is a former SomaLogic, Inc. (Boulder, CO, USA) employee and a company shareholder. O.H., Y.G.N., M.-D.W. and K.D.-N. are employees of Regeneron Pharmaceuticals Inc., a biopharma company. There are no conflicts of interest to report for the remaining coauthors.

## Additional information

**Extended data** is available for this paper at <https://doi.org/10.1038/s41590-020-00830-z>.

**Supplementary information** is available for this paper at <https://doi.org/10.1038/s41590-020-00830-z>.

**Correspondence and requests for materials** should be addressed to A.O. or M.J.L.

**Peer review information** *Nature Immunology* thanks Kevin Marchbank, Stuart Tangye and Chack-Yung Yu for their contribution to the peer review of this work. Peer reviewer reports are available. L. A. Dempsey was the primary editor on this article and managed its editorial process and peer review in collaboration with the rest of the editorial team.

**Reprints and permissions information** is available at [www.nature.com/reprints](http://www.nature.com/reprints).

Demographic and clinical features	P1		P2		P3		P4		P5		P6		P7		P8		P9		P10		P11		P12		P13		P14		P15		P16		
	Age	Sex	Age	Sex	Age	Sex	Age	Sex	Age	Sex	Age	Sex	Age	Sex	Age	Sex	Age	Sex	Age	Sex	Age	Sex	Age	Sex	Age	Sex	Age	Sex	Age	Sex	Age	Sex	
Age (years)	15	15	23	23	13	13	13	13	13	13	13	13	13	13	13	13	13	13	13	13	13	13	13	13	13	13	13	13	13	13	13	13	
Sex	M	F	M	F	M	F	M	F	M	F	M	F	M	F	M	F	M	F	M	F	M	F	M	F	M	F	M	F	M	F	M	F	
Current use (yr)	1	1	1	1	1	1	1	1	1	1	1	1	1	1	1	1	1	1	1	1	1	1	1	1	1	1	1	1	1	1	1	1	
Comorbidity	NA	NA	NA	NA	NA	NA	NA	NA	NA	NA	NA	NA	NA	NA	NA	NA	NA	NA	NA	NA	NA	NA	NA	NA	NA	NA	NA	NA	NA	NA	NA	NA	
Age at onset of symptoms (yr)	1	1	1	1	1	1	1	1	1	1	1	1	1	1	1	1	1	1	1	1	1	1	1	1	1	1	1	1	1	1	1	1	
Age at start of treatment (yr)	1	1	1	1	1	1	1	1	1	1	1	1	1	1	1	1	1	1	1	1	1	1	1	1	1	1	1	1	1	1	1	1	1
Time at follow-up (mo)	12	12	12	12	12	12	12	12	12	12	12	12	12	12	12	12	12	12	12	12	12	12	12	12	12	12	12	12	12	12	12	12	12
Peri-Tx	NA	NA	NA	NA	NA	NA	NA	NA	NA	NA	NA	NA	NA	NA	NA	NA	NA	NA	NA	NA	NA	NA	NA	NA	NA	NA	NA	NA	NA	NA	NA	NA	NA

**Extended Data Fig. 1 | Demographic, clinical and laboratory characteristics of the patients with CHAPLE disease enrolled in the study.** Reference ranges are indicated in parenthesis. NA: Not assessed, NP: New patient, WBC: White blood count, ANC: Absolute neutrophil count, ALC: Absolute lymphocyte count, Hgb: Hemoglobin, Plt: Platelet count. † CD55 NCBI Reference Sequence: [NM\\_00574](#). \* the lowest values in the past (more than 1 year before therapy) are indicated in the 'past' columns. \*\* the highest values in the past (more than 1 year before therapy) are indicated in the 'past' columns. The serum immunoglobulins compared to age-matched serum immunoglobulin reference ranges of Turkish children (Ref. 67). Peri-Tx: peri-treatment, referring to the past 12 months before the start of eculizumab until the end of the observation period.



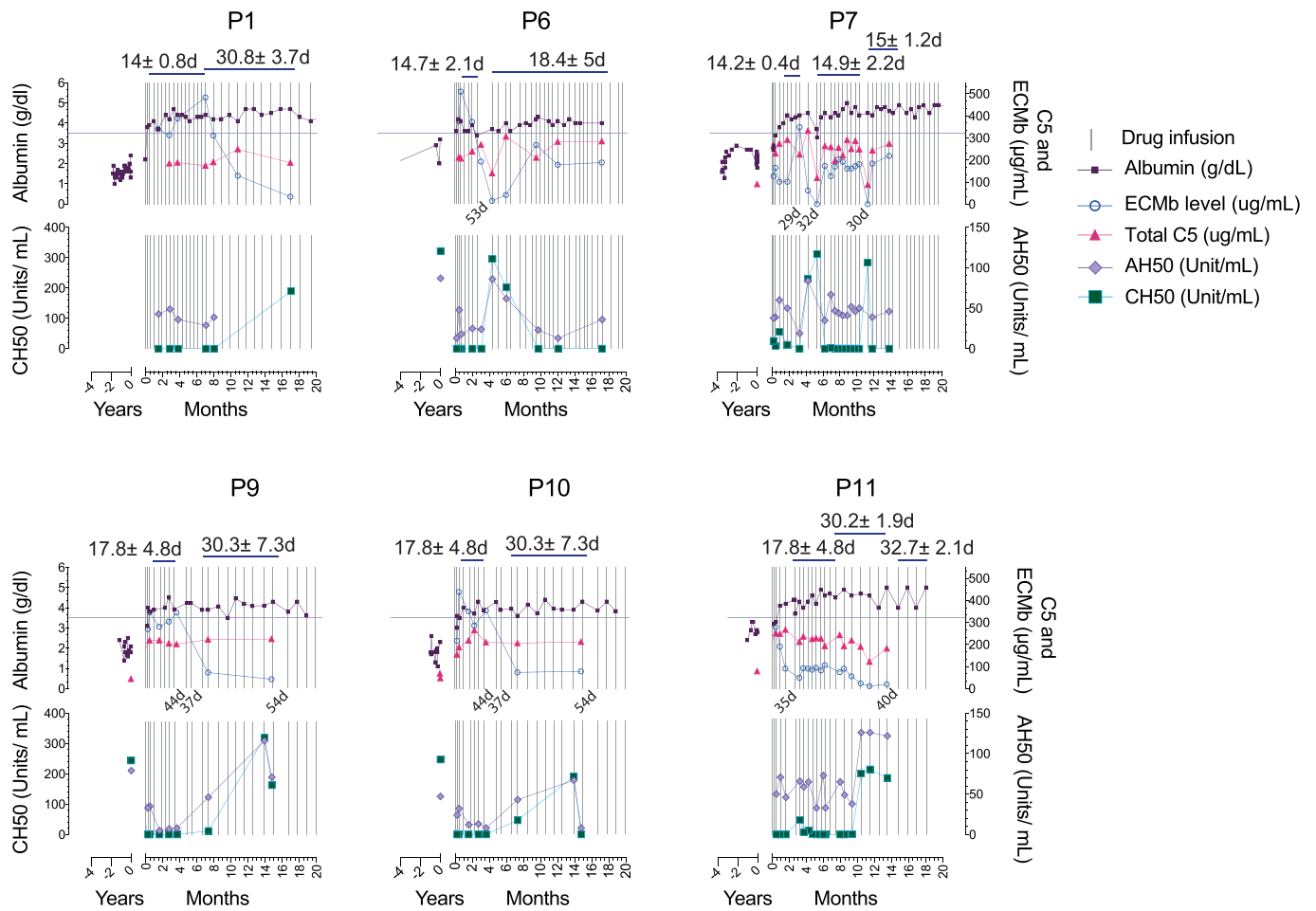
	P1	P2 §	P3	P4	P5	P6	P7	P8	P9	P10	P11	P12**	P13 †	P14 §	P15 §	P16			
	Peri-Tx	Peri-Tx	Peri-Tx	Peri-Tx	Peri-Tx	Peri-Tx	Peri-Tx	Peri-Tx	Peri-Tx	Peri-Tx	Peri-Tx	Peri-Tx	Peri-Tx	Peri-Tx	Peri-Tx	Peri-Tx			
	Past	Pre-tx	Current	Past	Pre-tx	Current	Past	Pre-tx	Current	Past	Pre-tx	Current	Past	Pre-tx	Current	Past	Pre-tx	Current	
Clinical features	Abdominal pain	+	+	+	+	+	+	+	+	+	+	+	+	+	+	+	+	+	
	Nausea	+	+	+	+	+	+	+	+	+	+	+	+	+	+	+	+	+	
	Vomiting	+	+	+	+	+	+	+	+	+	+	+	+	+	+	+	+	+	
	Diarrhea	+	+	+	+	+	+	+	+	+	+	+	+	+	+	+	+	+	
	Loss of appetite	+	+	+	+	+	+	+	+	+	+	+	+	+	+	+	+	+	
	Facial and/or extremity edema	+	+	+	+	+	+	+	+	+	+	+	+	+	+	+	+	+	+
	Albumin transfusion	+	+	+	+	+	+	+	+	+	+	+	+	+	+	+	+	+	+
	Thromboembolic disease ¶ †	-	-	-	-	-	-	-	-	-	-	-	-	-	-	-	-	-	-
	Thrombocytosis	+	+	+	+	+	+	+	+	+	+	+	+	+	+	+	+	+	+
	Bowel obstruction (acute remitting or persistent)¶	-	-	-	-	-	-	-	-	-	-	-	-	-	-	-	-	-	-
	Low albumin	+	+	+	+	+	+	+	+	+	+	+	+	+	+	+	+	+	+
	Low total protein	+	+	+	+	+	+	+	+	+	+	+	+	+	+	+	+	+	+
	Low IgG	+	+	+	+	+	+	+	+	+	+	+	+	+	+	+	+	+	+
	Low Vit B12	+	+	+	+	+	+	+	+	+	+	+	+	+	+	+	+	+	+
	Weight for age	≥ 50th percentile			x	x													
≥ 25th and <50th percentile			x																
≥ 10th and <25th percentile		x																	
≥ 3rd and <10th percentile		x	x																
< 3rd percentile																			
Stature for age	≥ 50th percentile			x	x														
	≥ 25th and <50th percentile																		
	≥ 10th and <25th percentile																		
	≥ 3rd and <10th percentile		x																
	< 3rd percentile	x	x	x															

**Extended Data Fig. 2 | Clinical symptoms, laboratory findings and growth percentiles of CHAPLE patients prior to and on ecizumab treatment.**

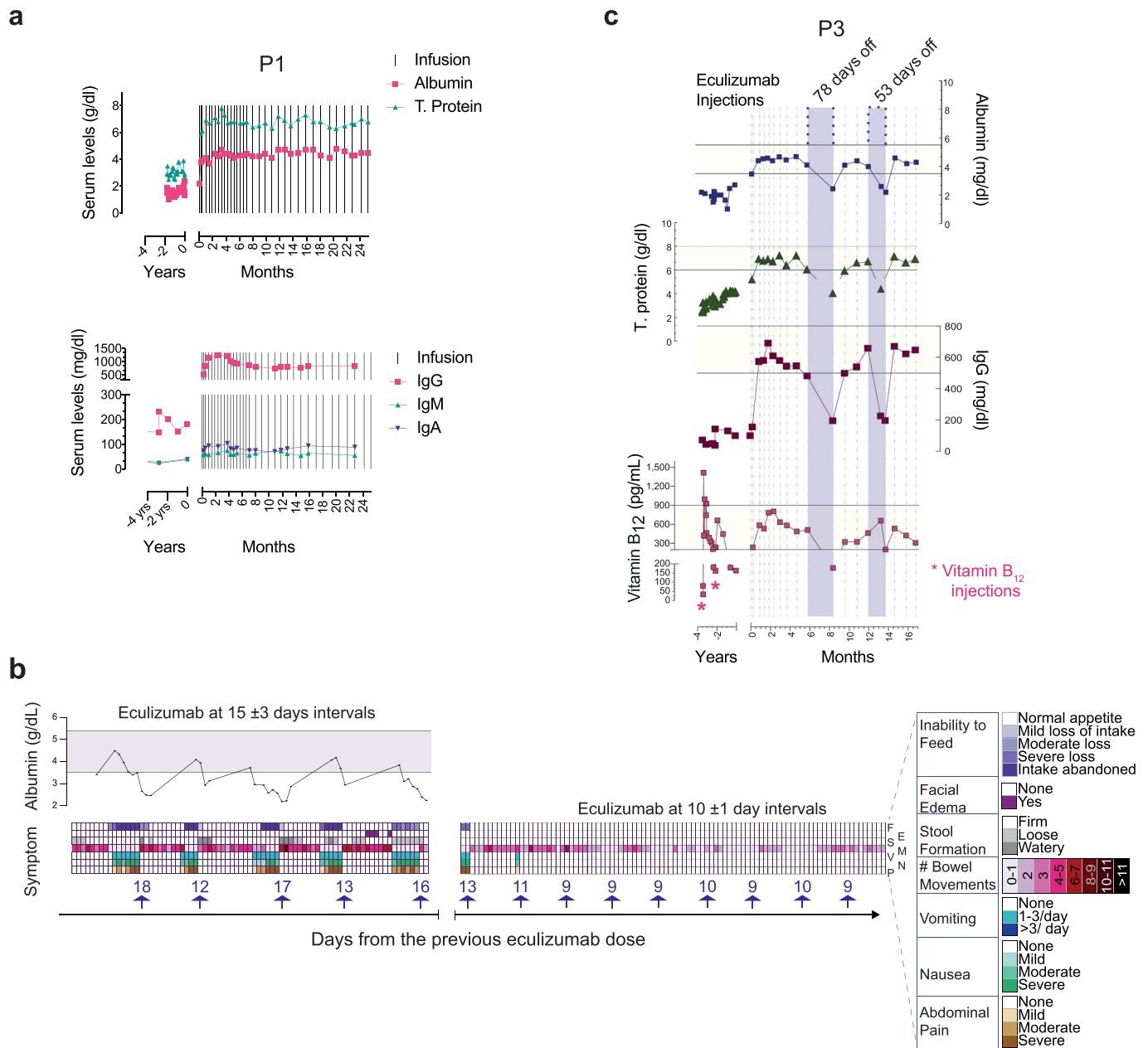
Past: In the lifetime of the patient. Peri-Tx: Peri-treatment, referring to the past 12 months before the start of ecizumab until the end of the observation period. Current refers to the most recent measurement or the observation period when a particular patient has been on regular ecizumab Tx. + present, - absent, N/A: Not assessed. ¶ We detected a recanalization of the narrowed segment in the thrombotic vessel in P5 during the follow up exam on ecizumab. However, there was no documented recovery of any of the thromboembolic complications in other patients during the indicated periods of follow up. \*\* P12 had ischemic gliotic foci in brain imaging. As identified by appropriate imaging including abdominal ultrasonography (USG) and/or doppler USG, and/or vascular imaging using a computed tomography or magnetic resonance imaging. § Growth percentiles not presented in certain columns; P2 was an adult during the peri-Tx period, and data not available in P14 and P15 for respective periods. † Abdominal pain cannot be assessed in P13 due to verbal immaturity and corresponding assessment was made for discomfort and abnormal crying behavior.

	P1		P2		P3		P4		P5		P6		P7		P8		P9		P10		P11		P12		P13 <sup>†</sup>		P14		P15		P16		
	Peri-Tx		Peri-Tx		Peri-Tx		Peri-Tx		Peri-Tx		Peri-Tx		Peri-Tx		Peri-Tx		Peri-Tx		Peri-Tx		Peri-Tx		Peri-Tx		Peri-Tx		Peri-Tx		Peri-Tx		Peri-Tx		
	Past	Current	Past	Current	Past	Current	Past	Current	Past	Current	Past	Current	Past	Current	Past	Current	Past	Current	Past	Current	Past	Current	Past	Current	Past	Current	Past	Current	Past	Current	Past	Current	
Bowel resection surgery*	-	-	-	-	-	-	-	-	-	-	-	-	-	-	-	-	-	-	-	-	-	-	-	-	-	-	-	-	-	-	-	-	
Other invasive interventions**	-	-	-	-	-	-	-	-	-	-	-	-	-	-	-	-	-	-	-	-	-	-	-	-	-	-	-	-	-	-	-	-	
Multivitamins	+	+	+	+	+	+	+	+	+	+	+	+	+	+	+	+	+	+	+	+	+	+	+	+	+	+	+	+	+	+	+	+	
Vit-D	+	+	+	+	+	+	+	+	+	+	+	+	+	+	+	+	+	+	+	+	+	+	+	+	+	+	+	+	+	+	+	+	
Vit B <sub>12</sub>	+	+	+	+	+	+	+	+	+	+	+	+	+	+	+	+	+	+	+	+	+	+	+	+	+	+	+	+	+	+	+	+	
Folate	+	+	+	+	+	+	+	+	+	+	+	+	+	+	+	+	+	+	+	+	+	+	+	+	+	+	+	+	+	+	+	+	
Iron	+	+	+	+	+	+	+	+	+	+	+	+	+	+	+	+	+	+	+	+	+	+	+	+	+	+	+	+	+	+	+	+	
Calcium, magnesium, zinc	+	+	+	+	+	+	+	+	+	+	+	+	+	+	+	+	+	+	+	+	+	+	+	+	+	+	+	+	+	+	+	+	
Omega-3 fatty acid	+	+	+	+	+	+	+	+	+	+	+	+	+	+	+	+	+	+	+	+	+	+	+	+	+	+	+	+	+	+	+	+	
MCT oil	-	-	-	-	-	-	-	-	-	-	-	-	-	-	-	-	-	-	-	-	-	-	-	-	-	-	-	-	-	-	-	-	
Enteral formula feeding	+	+	+	+	+	+	+	+	+	+	+	+	+	+	+	+	+	+	+	+	+	+	+	+	+	+	+	+	+	+	+	+	
Parenteral nutrition	-	-	-	-	-	-	-	-	-	-	-	-	-	-	-	-	-	-	-	-	-	-	-	-	-	-	-	-	-	-	-	-	
Erythrocyte transfusion	+	+	+	+	+	+	+	+	+	+	+	+	+	+	+	+	+	+	+	+	+	+	+	+	+	+	+	+	+	+	+	+	
Albumin transfusion	+	+	+	+	+	+	+	+	+	+	+	+	+	+	+	+	+	+	+	+	+	+	+	+	+	+	+	+	+	+	+	+	
Immunoglobulin Rx	+	+	+	+	+	+	+	+	+	+	+	+	+	+	+	+	+	+	+	+	+	+	+	+	+	+	+	+	+	+	+	+	
Corticosteroids	+	+	+	+	+	+	+	+	+	+	+	+	+	+	+	+	+	+	+	+	+	+	+	+	+	+	+	+	+	+	+	+	
Mesalazine	+	+	+	+	+	+	+	+	+	+	+	+	+	+	+	+	+	+	+	+	+	+	+	+	+	+	+	+	+	+	+	+	
Azathioprine	+	+	+	+	+	+	+	+	+	+	+	+	+	+	+	+	+	+	+	+	+	+	+	+	+	+	+	+	+	+	+	+	
Methotrexate	+	+	+	+	+	+	+	+	+	+	+	+	+	+	+	+	+	+	+	+	+	+	+	+	+	+	+	+	+	+	+	+	
Anti-TNF (Infliximab, adalimumab, cerolizumab)	+	+	+	+	+	+	+	+	+	+	+	+	+	+	+	+	+	+	+	+	+	+	+	+	+	+	+	+	+	+	+	+	
Low-molecular weight heparin	-	-	-	-	-	-	-	-	-	-	-	-	-	-	-	-	-	-	-	-	-	-	-	-	-	-	-	-	-	-	-	-	
Low dose acetyl salicylic acid	-	-	-	-	-	-	-	-	-	-	-	-	-	-	-	-	-	-	-	-	-	-	-	-	-	-	-	-	-	-	-	-	
TPA lysis of clots	-	-	-	-	-	-	-	-	-	-	-	-	-	-	-	-	-	-	-	-	-	-	-	-	-	-	-	-	-	-	-	-	
Respiratory support §	-	-	-	-	-	-	-	-	-	-	-	-	-	-	-	-	-	-	-	-	-	-	-	-	-	-	-	-	-	-	-	-	
Ocrototide to alleviate PLE	+	+	+	+	+	+	+	+	+	+	+	+	+	+	+	+	+	+	+	+	+	+	+	+	+	+	+	+	+	+	+	+	
Antibiotic prophylaxis	+	+	+	+	+	+	+	+	+	+	+	+	+	+	+	+	+	+	+	+	+	+	+	+	+	+	+	+	+	+	+	+	
IV antibiotics/ Tx for unusual infections †	+	+	+	+	+	+	+	+	+	+	+	+	+	+	+	+	+	+	+	+	+	+	+	+	+	+	+	+	+	+	+	+	
Thyroxin for hypothyroidism	+	+	+	+	+	+	+	+	+	+	+	+	+	+	+	+	+	+	+	+	+	+	+	+	+	+	+	+	+	+	+	+	+

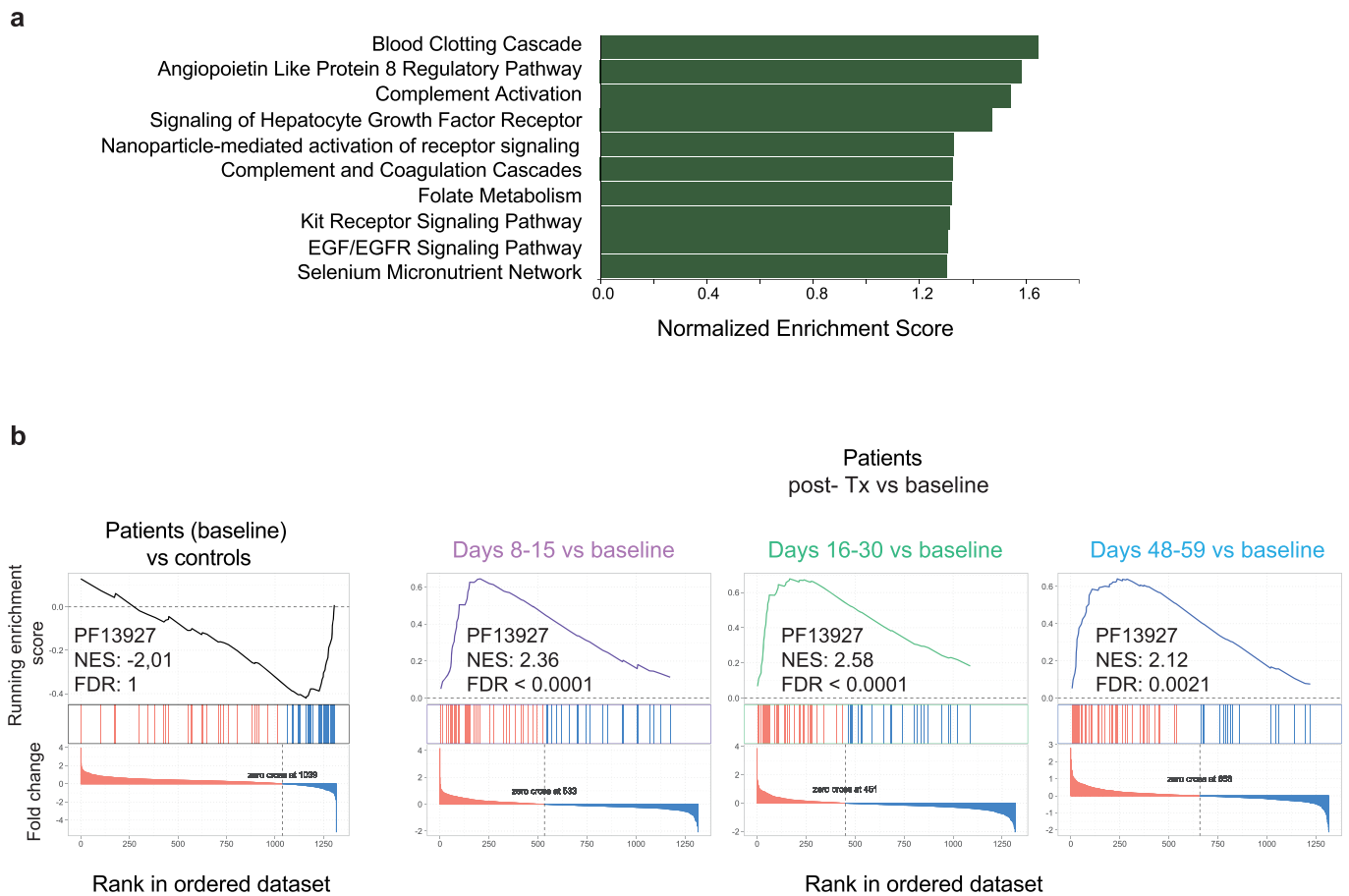
**Extended Data Fig. 3 | Medical interventions received by CHAPLE patients prior to and during ecilizumab treatment.** Past: In the lifetime of the patient. Peri-Tx: Peri-treatment, referring to the past 12 months before the start of ecilizumab until the end of the observation period. Current refers to the most recent measurement or the presence of a finding during the observation period when a particular patient has been on regular ecilizumab Tx. \*A repeat bowel surgery had been planned in P8 prior to ecilizumab. Likewise, P3 had been planned to undergo bowel surgery before ecilizumab. P15 underwent 2 separate bowel resection surgeries and received 39 days of intensive care support during the postoperative period, including mechanical ventilation. \*\* 'Other invasive intervention' includes placement of a central access device in P8 to deliver frequent albumin transfusions; intracardiac blood clot removal surgery, chest tube placement to drain pneumothorax and a cranial surgery to alleviate brain hemorrhage in P4; a percutaneous endoscopic gastrostomy port to support enteral nutrition in P12; a transjugular intrahepatic portosystemic shunt (TIPS) to relieve portal hypertension in P16. † P8 received intravenous (IV) antibiotics for sepsis and metronidazole for Giardia lamblia enteritis in the past. P4 and P12 experienced cardiovascular problems during the induction period of ecilizumab, leading to dose skipping or termination of treatment, respectively. Ecilizumab Tx was restarted in P12 after a period off- therapy, with no recurrence of similar manifestations. Fecal assessment during diarrheal episodes revealed Cryptosporidium parvum in P1 and P13 prior to ecilizumab, who were treated with nitazoxanide uneventfully. The column for past medication before 1 year prior to ecilizumab is blank for P13 due to young age and onset of symptoms during the past year. § Respiratory support refers to mechanical ventilation and/or oxygen treatment. PLE: Protein-losing enteropathy.



**Extended Data Fig. 4 | The effect of dose spacing between injections on albumin, trough ecuzimab concentration, and complement markers during the maintenance therapy.** Blood samples were obtained prior to each injection. The horizontal line on left y axis shows lower range for albumin. Calculated mean  $\pm$  S.D. values for dose intervals during the indicated time spans, or between two consecutive injections are presented in days. ECMb: ecuzimab.



**Extended Data Fig. 5 | Variable dose spacing or interrupted therapy. a.** Normal serum protein levels sustained when switching from biweekly doses to monthly eculizumab injections in P1. Timing of eculizumab doses in relation to serum albumin and total protein concentrations for P1 in top panel, and immunoglobulin isotypes IgG, IgM and IgA in the bottom panel. **b.** Timeline plotting the incidence and severity of the indicated symptoms in P4 in relation to timing of eculizumab injection at various dosing intervals. Serum albumin levels plotted at the top of the figure with the horizontal bar showing normal range. Each arrow above the x-axis shows an eculizumab injection with the accompanying numbers illustrating days from the previous dose. The top line shows inability to feed (F) ranging from normal appetite (white) to intake completely abandoned (dark purple). The second line shows the presence (purple) or absence (white) of facial edema (E) in purple whereas the third line shows stool formation (S) on a scale from firm (white) to watery (dark gray). The fourth line quantifies the number of bowel movements (M) from 0-1 (white) to >11 (black). The fifth and sixth lines show the incidences of vomiting (V) from none (white) to >3 times per day (dark blue) and severity of nausea (N) from none (white) to severe (green), respectively. The last line shows severity of abdominal pain (P), ranging from none (white) to severe (dark brown). **c.** Serum albumin, total protein (T. protein), immunoglobulin G (IgG), and vitamin B<sub>12</sub> concentrations for P3 before and after treatment at t=0. Horizontal yellow bars for indicated parameters show normal range. Vertical dashed lines show eculizumab injections and purple bars dose skipping periods with the indicated numbers showing intervals between two consecutive injections.



**Extended Data Fig. 6 | Biological significance of proteomic changes in serum. a**, Top-ranking pathways (Wikipathways) plotted against normalized enrichment score (Ref. <sup>68,69</sup>). Note, the enrichment of the pathways did not reach adjusted statistical significance level of false discovery rate (FDR) < 0.05. **b**, Enrichment plots from pre-ranked analysis of  $\log_2$  fold changes (FC) in protein abundances of patients with respect to age-matched controls, showing rank-based ordering of proteins belonging to immunoglobulin Pfam domain PF13927 at baseline. Similar plots are generated for indicated Post-treatment (Post-Tx) timepoints using  $\log_2$  FC in protein abundances calculated with respect to patient baseline values. PF13927, found to be enriched in the STRING analysis (Ref. <sup>70</sup>), was added to the Wikipathways gene set to compute the normalized enrichment score (NES) and FDR.

## Reporting Summary

Nature Research wishes to improve the reproducibility of the work that we publish. This form provides structure for consistency and transparency in reporting. For further information on Nature Research policies, see our [Editorial Policies](#) and the [Editorial Policy Checklist](#).

### Statistics

For all statistical analyses, confirm that the following items are present in the figure legend, table legend, main text, or Methods section.

n/a Confirmed

- The exact sample size ( $n$ ) for each experimental group/condition, given as a discrete number and unit of measurement
- A statement on whether measurements were taken from distinct samples or whether the same sample was measured repeatedly
- The statistical test(s) used AND whether they are one- or two-sided  
*Only common tests should be described solely by name; describe more complex techniques in the Methods section.*
- A description of all covariates tested
- A description of any assumptions or corrections, such as tests of normality and adjustment for multiple comparisons
- A full description of the statistical parameters including central tendency (e.g. means) or other basic estimates (e.g. regression coefficient) AND variation (e.g. standard deviation) or associated estimates of uncertainty (e.g. confidence intervals)
- For null hypothesis testing, the test statistic (e.g.  $F$ ,  $t$ ,  $r$ ) with confidence intervals, effect sizes, degrees of freedom and  $P$  value noted  
*Give  $P$  values as exact values whenever suitable.*
- For Bayesian analysis, information on the choice of priors and Markov chain Monte Carlo settings
- For hierarchical and complex designs, identification of the appropriate level for tests and full reporting of outcomes
- Estimates of effect sizes (e.g. Cohen's  $d$ , Pearson's  $r$ ), indicating how they were calculated

*Our web collection on [statistics for biologists](#) contains articles on many of the points above.*

### Software and code

Policy information about [availability of computer code](#)

Data collection

Data analysis

For manuscripts utilizing custom algorithms or software that are central to the research but not yet described in published literature, software must be made available to editors and reviewers. We strongly encourage code deposition in a community repository (e.g. GitHub). See the Nature Research [guidelines for submitting code & software](#) for further information.

### Data

Policy information about [availability of data](#)

All manuscripts must include a [data availability statement](#). This statement should provide the following information, where applicable:

- Accession codes, unique identifiers, or web links for publicly available datasets
- A list of figures that have associated raw data
- A description of any restrictions on data availability

## Field-specific reporting

Please select the one below that is the best fit for your research. If you are not sure, read the appropriate sections before making your selection.

Life sciences       Behavioural & social sciences       Ecological, evolutionary & environmental sciences

For a reference copy of the document with all sections, see [nature.com/documents/nr-reporting-summary-flat.pdf](https://www.nature.com/documents/nr-reporting-summary-flat.pdf)

## Life sciences study design

All studies must disclose on these points even when the disclosure is negative.

Sample size	This study involves human subjects with an ultra-rare disease. No priori sample size calculation was made; prospective subjects who meet inclusion criteria were enrolled upon consenting to the study.
Data exclusions	There were no data exclusions in the study.
Replication	Different patients with individual genetic backgrounds serve as biological replicates for a given measurement. Moreover, each patient was tested for multiple times prior to- and following- treatment initiation; all data showed consistent trends during the repeated analyses for given time periods. We also measured certain markers using various methods; each time one study recapitulated the finding generated using a different methodology. For example, in the proteome study we selected one of the discovered biomarkers (IGFBP2) to validate the results using a different assay. ELISA was able to replicate the finding. The soluble CD55 measurement for Patient 12 and her father was studied on different runs using separate blood draws and recapitulated the reported data at every examination.
Randomization	Treatment randomization not applicable since this is not a randomized clinical study. For the experimental studies biological sample collection was requested from all patients enrolled. Since there was no subgroup allocation for a particular experiment, no randomization was required.
Blinding	The researchers who carried pharmacokinetic and pharmacodynamic examinations were blinded to the study subjects since each sample tube was labeled with a code that included no metadata. For the proteomic and metagenomic studies the technicians who analyzed the samples were blinded to the group allocation information. The bioinformaticians carried the computational analyses by matching the sample metadata with the experimental test results, each provided by independent researchers. The bioinformatician who analyzed whole genome sequencing data was blinded to serum C4 values when calculating estimated C4 gene copy numbers but not blinded to patient allocation when searching for C5 gene variants, since the latter analysis required appropriate filtering strategies.

## Reporting for specific materials, systems and methods

We require information from authors about some types of materials, experimental systems and methods used in many studies. Here, indicate whether each material, system or method listed is relevant to your study. If you are not sure if a list item applies to your research, read the appropriate section before selecting a response.

### Materials & experimental systems

n/a	Involved in the study
<input type="checkbox"/>	<input checked="" type="checkbox"/> Antibodies
<input checked="" type="checkbox"/>	<input type="checkbox"/> Eukaryotic cell lines
<input checked="" type="checkbox"/>	<input type="checkbox"/> Palaeontology and archaeology
<input checked="" type="checkbox"/>	<input type="checkbox"/> Animals and other organisms
<input type="checkbox"/>	<input checked="" type="checkbox"/> Human research participants
<input checked="" type="checkbox"/>	<input type="checkbox"/> Clinical data
<input checked="" type="checkbox"/>	<input type="checkbox"/> Dual use research of concern

### Methods

n/a	Involved in the study
<input checked="" type="checkbox"/>	<input type="checkbox"/> ChIP-seq
<input type="checkbox"/>	<input checked="" type="checkbox"/> Flow cytometry
<input checked="" type="checkbox"/>	<input type="checkbox"/> MRI-based neuroimaging

## Antibodies

Antibodies used	Purified mouse APC-conjugated anti-human CD3 antibody (BD, catalog # 347340, clone SK7), Purified mouse PERCP-conjugated anti-human CD19 antibody (BD, catalog # 347540, clone 4G7), Purified mouse PE-conjugated anti-human CD55 antibody (BioLegend, catalog # 311302, clone JS11). Cytometric Bead Array (CBA) Human Anaphylatoxin Kit (BD, catalog # 561418). Ruthenium labeled anti-C5 antibody developed in house (Regeneron Pharmaceuticals). MicroVue sC5b-9 Plus EIA kit (Quidel Corporation, Catalogue # A020) DuoSet ELISA kit to measure IGFBP2 (R&D Systems, Catalogue # DY674)
Validation	Each primary antibody was validated by the manufacturers. Previous publications that employed these antibodies include: 1. Anti-human CD3 antibody: Campbell et al. Doi: 10.1007/s10549-004-7048-0), 2. Anti-human CD19 antibody: Bloomfield et al. Doi: 10.1056/NEJM197909063011002. 3. Anti-human CD55 antibody: Peyron et al. Doi: 10.4049/jimmunol.165.9.5186. 4. Anti-human sC5b-9 antibody: Noris et al. doi: 10.1182/blood-2014-02-558296. 5. Anti-human IGFBP2

## Human research participants

Policy information about [studies involving human research participants](#)

Population characteristics	The studied population consisted of children or young adults reflecting the typically presenting age of CHAPLE disease. This disease follows an autosomal recessive inheritance pattern in which both sexes are equally affected; there was no gender-bias in our study. We studied 16 caucasian patients (9 females and 7 males; mean age: 17.9 years; S.D: 5.5 years) from 14 unrelated families harboring a range of genetic lesions in the CD55 gene as specified in the manuscript. The median follow-up duration was 20 months (interquartile range 18 to 22 months).
Recruitment	We invited prospective CHAPLE subjects who were planned to receive eculizumab treatment or already on this medication. Eligible subjects carrying no exclusion criterion were included upon consenting to the study protocol. Since only active patients were treated with eculizumab this may introduce a bias towards inclusion of more severe cases over those with milder disease. It is possible that the discovered metabolic, immune, and microbiome changes in our study may not reflect the changes in milder patients. Also, some aspects of the natural history of the disease presented in this paper may be different than the overall CHAPLE population that includes milder subjects.
Ethics oversight	Marmara University Medical Faculty Institutional Review Board for Clinical Researches ( <a href="https://tip.marmara.edu.tr/en/ethics-committee">https://tip.marmara.edu.tr/en/ethics-committee</a> ) approved the study protocol.

Note that full information on the approval of the study protocol must also be provided in the manuscript.

## Flow Cytometry

### Plots

Confirm that:

- The axis labels state the marker and fluorochrome used (e.g. CD4-FITC).
- The axis scales are clearly visible. Include numbers along axes only for bottom left plot of group (a 'group' is an analysis of identical markers).
- All plots are contour plots with outliers or pseudocolor plots.
- A numerical value for number of cells or percentage (with statistics) is provided.

### Methodology

Sample preparation	We used peripheral blood from the study subjects for CD55 surface staining. The processing of blood and the staining procedure are described in the methods. Plasma anaphylatoxins C3a, C4a, and C5a were measured using a flow cytometry based cytometric bead array.
Instrument	FACS Calibur (Becton Dickinson, USA) was used for the surface staining of cells for CD55. Anaphylatoxin measurements were performed on a Navios EX flow cytometer (Beckman Coulter, France)
Software	Flow Jo v. X
Cell population abundance	Histograms of the CD55 fluorescence from patient cells were overlaid with the isotype controls and healthy controls to determine reduced expression.
Gating strategy	Gating strategy for CD55 assessment and the anaphylatoxin measurement in plasma is summarized in Supplementary Fig. 1. Briefly, lymphocytes were gated in FSC-A vs SSC-A plots, followed by gating on CD3+CD19- cells, which were clearly separated from the other cell populations. Then, histogram plots for CD55 were created. To assess anaphylatoxin C3a, C4a, and C5a concentrations in plasma, a gating from the beads was followed by assessment of MFI values from the corresponding clusters for each analyte as recommended by the manufacturer.

- Tick this box to confirm that a figure exemplifying the gating strategy is provided in the Supplementary Information.